math xmlns="http://www.w3.org/1998/Math/MathML">mrow>mmultiscripts>mi mathvariant="normal">Cr/mi>mprescripts>/mprescripts>none>/none>mn>53/mn>/mmultiscripts>/mrow>/math> solid-state nuclear magnetic resonance: New observations and comprehensive correlations as a probe of valence and magnetic states

Timothy J. Bastow, Anita J. Hill, Katherine M. Nairn, and Mark E. Smith

Phys. Rev. Materials **7**, 114410 — Published 27 November 2023

DOI: 10.1103/PhysRevMaterials.7.114410

^{53}Cr Solid-State Nuclear Magnetic Resonance: New Observations and Comprehensive Correlations as a Probe of Valence and Magnetic States

Timothy J. Bastow[1], Anita J. Hill[1*], Katherine M. Nairn[2], and Mark E. Smith[3*]

[1]CSIRO Manufacturing, Stewart Bastow Building, Clayton, Victoria, 3168 Australia

[2]Department of Materials Engineering, Monash University, Victoria, 3800, Australia

[3]Vice-Chancellor and President's Office and Department of Chemistry, University of Southampton, Southampton SO17 1BJ, UK.

*corresponding authors: anita.hill@csiro.au m.e.smith@soton.ac.uk

ORCID

T. J. Bastow 0000-0002-3743-9434

A. J. Hill 0000-0003-1574-243X

K. M. Nairn

M. E. Smith 0000-0002-6254-6792

Abstract

New ^{53}Cr solid-state NMR measurements are presented for Cr_2N, CrB_2, CrO_2, Cr_2O_3, $(NH_4)_2CrO_4$, and $BaCrO_4$. Measurements of the ^{53}Cr nuclear quadrupole coupling constants, asymmetry parameters, and chemical (Knight) shifts of chromium compounds provide important experimental data for the validation of quantum chemistry calculations. In this work, natural abundance ^{53}Cr magnetic resonance, at 9.4 T, is used to examine the metals Cr_2N and CrB_2 as well as the diamagnetic insulating chromates $(NH_4)_2CrO_4$ and $BaCrO_4$ at room temperature. ^{14}N and ^{11}B NMR spectra are also obtained at room temperature for Cr_2N and CrB_2, respectively. The shift observed from CrB_2 is believed to be the largest Cr(0) Knight shift (–9982 ppm) for any chromium-containing metallic material. ^{53}Cr measurements in zero applied magnetic field as a function of temperature are reported for ferromagnetic CrO_2 and antiferromagnetic Cr_2O_3. Within experimental accuracy the magnetization behavior in CrO_2 is modelled using Bloch spin wave theory where the magnetization decreases as $T^{3/2}$ over temperatures from 4.2 to 295 K, which also appears to adequately model the sublattice magnetization of Cr_2O_3. These new experimental results are put into the context of previous magnetic resonance results found in the literature by providing the first comprehensive tabulation of such ^{53}Cr magnetic resonance data from solids for over 50 years. The low temperature zero applied magnetic field central frequencies are correlated with valence state, and spin stiffness has been calculated for sixteen chromium compounds. A knowledge of these parameters will enable further progress in using ^{53}Cr magnetic resonance as a probe of electronic and magnetic structures thereby contributing to the more systematic development of novel materials.

Keywords: chromium, NMR, zero applied field, magnetic hyperfine interactions, quadrupolar, shifts, spin waves

1. Introduction

^{53}Cr NMR studies of solid chromium-containing compounds were first reported in the 1960s as research teams sought to unravel the nature of the bonding in antiferromagnetic and ferromagnetic materials and to test theoretical schemes for approximating the nature of magnetic ordering [1-5]. With the current level of interest in quantum materials, for applications in spintronics and as topological insulators, the challenge of understanding, predicting, and controlling magnetic properties and quantum states in Cr compounds has reinvigorated ^{53}Cr NMR studies [6-8]. The literature of relevance to the compounds studied here for the first time is introduced, followed by a report of new measurements of ^{53}Cr NMR at 9.4 T and in zero applied field with ^{53}Cr in natural abundance. These new results are compared with the literature where the ability to understand the valence and magnetic environment are highlighted. A key aim here is to provide a comprehensive overview of the literature on ^{53}Cr magnetic resonance from 1961 to date. The implications for the trends in these data and the ability to probe bonding and spin properties for correlation with other materials properties (e.g. magnetization, spin density) are examined. Suggestions for future work are highlighted throughout the results and discussion.

2. State-of-the-art of magnetic resonance observation of chromium in solids

The first report of solid-state ^{53}Cr (I=3/2, natural abundance 9.5%) NMR was in ferromagnetic $CrBr_3$ by Gossard *et al*. [1]. The NMR lineshape could be obtained in zero applied field because of the existence of a strong internal magnetic hyperfine field at the Cr nucleus at temperatures below the ferromagnetic Curie point temperature T_C = 37 K. Using the internal field in materials with spontaneous magnetization to observe the magnetic resonance signal is termed zero field NMR or ferromagnetic nuclear resonance (FNR). The temperature dependence of the ^{53}Cr resonance was measured from 1.34 to 4.2 K, and the data were fitted with spin wave theory [9-11]. These ^{53}Cr NMR results were the first experimental test of spin wave theory for a ferromagnetic compound using NMR. Three months after the Gossard *et al.* report [1], Narath [2] reported the first zero field ^{53}Cr NMR in an antiferromagnetic compound, $CrCl_3$ (Néel temperature, T_N = 16.8 K) measured from 1.23 to 4.02 K, providing data for a further test of spin wave theory. The ferromagnet CrI_3 (T_C = 68 K) was subsequently characterized using ^{53}Cr zero field NMR as a low temperature test of spin wave theory [3]. Anisotropic Cr orbital states form a current topic of materials research interest for spintronic devices, and as such the chromium trihalides are still under investigation experimentally and theoretically as 2D materials with intrinsic ferromagnetic and antiferromagnetic properties [12,13].

Rubinstein *et al.* [14] studied ^{53}Cr in antiferromagnetic Cr_2O_3 in zero applied field using powder samples with ^{53}Cr in natural abundance and enriched. For measurements at 1.6 K, the central line was detected at 70.43 MHz with the satellite transitions lying 262±10 kHz to either side, yielding a quadrupolar frequency ν_Q of 0.525 MHz and a quadrupole coupling constant C_Q of 1.05 MHz for Cr_2O_3 (ν_Q and C_Q defined in Section 4.1). The central line resonance frequency was reported as constant within the accuracy of the measurement over the temperature range studied from 1.6 to 16 K. To date no one has reported ^{53}Cr NMR measurements of Cr_2O_3 at temperatures much above liquid helium temperature. Internal field magnetic resonance data are reported in the present work, significantly extending the temperature range.

The first report of ^{53}Cr NMR in ferromagnetic CrO_2 was in 1963 by Yasuoka *et al.* [15] who detected a single peak at 36.14 MHz in zero field at 77 K with the weak signal disappearing

above 240 K. A later study [16] at 4.2 K and zero applied field reported two ^{53}Cr peaks at 26.3 and 36.7 MHz, even though a single chromium site is expected in the rutile structure of stoichiometric highly crystalline CrO_2; the authors tentatively attributed the high frequency line to the expected single Cr site and the low frequency line to Cr atoms affected by vacancies. The origin of these two ^{53}Cr sites has continued to be the subject of study. In 2007 Shim *et al.* [17] showed that the sites could not be due to vacancies, nor could they be due to Cr sites in domains and domain walls. Much recent work has been reported on ^{53}Cr in CrO_2 due to renewed interest in anomalous electronic states of half metallic chromium oxides [18-21], with the most robust recent attribution of the two sites to an electronic state caused by local orbital order [18-20].

^{53}Cr NMR measurements in numerous diamagnetic chromates have been reported with nuclear quadrupolar coupling constants, C_Q, ranging from 1.17 to 5.01 MHz for eleven chromates and 7.25 to 8.28 MHz for two dichromates [22-24]. The ^{53}Cr chemical shift range reported in diamagnetic alkali earth chromate and dichromate compounds is −117 ppm to +188 ppm attributed to the small shielding anisotropies expected for d^0 Cr(VI) complexes [22,25]. Nowak and co-authors [26,27] have reported ^{53}Cr NMR in hexagonal and cubic chromium hydrides, establishing these compounds as metals (Pauli paramagnets) and reporting the temperature independent Knight shift for each phase. Barnes and Graham determined the Knight shift in pure Cr metal in the paramagnetic state above T_N = 313 K and at 300 K in $Cr_{1-x}V_x$ alloys with up to 3 at% V [6]. Kontani [28] reported ^{53}Cr NMR for the $Cr_{1-x}Mo_x$ system with x varying from 0.25 to 26.3 at%. Although there are several important Cr-containing stoichiometric compounds that are metals, e.g. the chromium boride refractory metals and the chromium nitrides, to date there has been very little ^{53}Cr NMR reported in metals and alloys [29-31]. ^{53}Cr has a nuclear gyromagnetic ratio, γ, of −2.406 MHz/T which is low [29], and ^{53}Cr is not the most favored of the low-γ nuclides for solid-state NMR, sometimes being referred to as exotic, miscellaneous, unreceptive, and difficult. However, it has been shown in recent years that a combination of relatively large samples and, for wide lines, techniques such as frequency stepping can aid in the observation of low-γ nuclei [24,29,30,32], helping to overcome the challenges of low sensitivity, low natural abundance, and broad resonance lines. This study encompasses a wide range of samples some of which will have high internal magnetic fields or large Knight shifts which can produce a large fluctuating spin density/magnetic field at the ^{53}Cr site resulting in short T_1 relaxation times. In other samples, (e.g. non-magnetic insulating samples) the relaxation can be significant slower. Typically, the recycle delays were set to produce relaxed or partially relaxed spectra tailored to the sample. In most samples fast relaxation occurs so a repetition time of 20-100 ms was used. The ability to recycle quickly for most samples means spectra can be rapidly collected helping the observation, especially when frequency-stepping strategies are adopted to locate the resonances by looking over a large frequency range. In addition, for ferro- and ferrimagnetic samples, the way the electronic magnetization responds to the applied rf field can lead to a very significant additional boost to the magnitude of the signal through the enhancement mechanisms operating [33,34].

3. Experimental details

CrO_2 and CrB_2 powders (99% purity), Cr_2O_3 and $BaCrO_4$ powders (purity ≥ 98%), and $(NH_4)_2CrO_4$ powder (98% purity) were obtained from Sigma Aldrich. Industrial grade Cr_2N powder (92% purity) was obtained from Japan. Powder X-ray diffraction (XRD) scans were

measured using a Bruker D8 Advance spectrometer using Cu Kα radiation to confirm crystallinity and purity. Analysis of the data was performed using the Bruker XRD search match program EVA™4.2. Differential scanning calorimetry (DSC) was performed on 10 mg of the Cr_2O_3 powder using a Mettler Toledo DSC 2 at a heating rate of 10 K/min from 133 to 373 K in flowing nitrogen (40 mL/min). Analysis of the data was performed using the STAR^e software. A Zeiss Merlin field emission scanning electron microscope (SEM) was used to acquire images of the CrO_2 powder at an accelerating voltage of 3 kV and 100,000x magnification.

High field (9.4 T) and zero applied field NMR spectroscopy were performed using a Bruker Avance 400 spectrometer to generate the pulses and detect the signal via a phase-cycled two pulse echo sequence using a pulse duration of ~4 to 10 μs, pulse separation of ~50 μs, and pulse repetition time of 20 to 500 ms depending on nuclear relaxation rate. The Larmor resonance frequencies for the investigated nuclei ^{11}B, ^{14}N, and ^{53}Cr at B_0 = 9.4 T are 128.40, 28.91, and 22.66 MHz, respectively. The reference ^{11}B NMR zero line shift was set using $NaBH_4$ in dilute aqueous solution; the reference for ^{14}N was solid NH_4Cl; the reference for ^{53}Cr was $(NH_4)_2CrO_4$ in saturated aqueous (D_2O) solution. For CrO_2, small low power 1 μs pulses were used since the signal strength is boosted by the inter- and intra-domain signal enhancement mechanism in ferromagnets described elsewhere [33,34]. There was not a systematic determination here of the enhancement factor, although for ^{53}Cr, the core domains (as opposed to the domain walls) where it is reported in the papers summarized here, the enhancement factor is usually in the range 10-100 and typically around 30. The probe bandwidth was approximately 800 kHz (full width at half maximum (fwhm) of the tuning curve). The ^{53}Cr zero field NMR lines were recorded at 77, 195, and 295 K at an operating frequency adjusted to put the line maximum at the center of the frequency range. Frequency-stepped spectra [32] for ^{53}Cr were obtained at 295 K for CrB_2 and Cr_2N at 9.4 T and at 77 and 195 K in zero field for Cr_2O_3. For the lines defined by frequency stepping, the width of the pulses was varied to achieve the pulse bandwidth for the chosen frequency slice: typically, 5 μs for a 200 kHz slice using 300 W transmitter power. For Cr_2O_3 higher power 5 μs pulses were necessary since the signal enhancement mechanism that operates for ferromagnets is not applicable to antiferromagnets. The probe head was an 8 cm long cylindrical copper pot with an enamelled wire wound coil attached to a home-built matching circuit by a short, low thermal conductivity, transmission line [35].

4. Results and discussion

4.1 Hyperfine interactions

Hyperfine interactions experienced by a nucleus act as fingerprints of the different atomic sites in materials. In the case of the compounds examined here, the parameters determined by magnetic resonance measurements provide a sensitive probe of the local and magnetic structure around the ^{53}Cr atomic sites. The interactions experienced by a ^{53}Cr nucleus include quadrupolar via electric field gradients (efgs), shielding (either chemical shift from conventional localized electronic bonding or Knight shift from delocalized conduction electrons), and for electronic magnetism, the local internal field [29,30,33,34]. An atomic nucleus with spin I > 1/2 has an electrical quadrupole moment which interacts with any efg, whose largest component V_{zz} (J/Cm^2) is defined as

$$V_{zz} = \partial^2 V/\partial z^2 \qquad \text{(Eq. 1)}$$

Simulation of the lineshape features can give the nuclear quadrupole coupling constant, C_Q, in units of frequency and asymmetry parameter η, defined as

$$C_Q = eQV_{zz}/h \text{ and } \eta = (V_{xx}-V_{yy})/V_{zz} \quad \text{(Eq. 2)}$$

where Q is the quadrupole moment of the nucleus in units m^2, e is the electron charge in units of Coulomb (C), h is Planck's constant and V_{ii} are the respective efg tensor components. In highly crystalline, well-ordered samples the resulting powder lineshapes of all transitions will be structured with clear peaks and singularities from which the quadrupolar interaction parameters can be extracted [29,30]. Often such structure cannot be observed, in which case the second-order perturbed central line width Δ (fwhm) can be used to estimate C_Q via [29,30]:

$$\Delta = (25(\nu_Q^2)/144\ \nu_L)\ (I(I+1)-3/4), \text{ where } \nu_Q = 3C_Q\ [\sqrt{(1+(\eta^2/3))}]/(2I(2I-1)) \quad \text{(Eq. 3)}$$

and where ν_L is the Larmor frequency. The value of C_Q from experiment can be compared with the V_{zz} calculated from density functional theory (DFT). This combination of spectroscopic measurement and quantum chemistry calculations of quadrupole parameters provides a powerful means to study the solid state (see for example Bastow *et al.* [36]).

Recently, DFT methods have also been used to calculate the magnetic shielding or hyperfine induced shift of the nuclear resonance (Knight shift, KS) in elemental metals [37] using the Wien2k program [38] where both orbital and spin contributions are needed for the transition metals. For ^{53}Cr in pure Cr metal, the theoretical KS of 6818 ppm is in excellent agreement with the experimental KS of 6870 ± 100 ppm [4,37]. Where possible in this study, measured values for C_Q and chemical (Knight) shift are compared to DFT predictions for these values. For Cr compounds with spontaneous magnetization, the Knight shift (in %) is related to the Pauli spin susceptibility χ_P per Cr atom (in cm^3/mol) by

$$KS = [A][\ \chi_P\ /(N_A\mu_B)] \quad \text{(Eq. 4)}$$

where A is the hyperfine coupling constant in T/μ_B, N_A is Avogadro's number $6.022\text{x}10^{23}$ mol^{-1} and $\mu_B = 9.27\text{x}10^{-24}$ J/T.

When there are unpaired electrons then an internal magnetic field is generated and usually no magnetic field needs be applied. The zero field applied NMR (zf) center-line resonance, ν_{zf}, (in units of MHz) is a measure of the hyperfine field at the ^{53}Cr nucleus, B_{hf} (in units of T) through the relationship

$$B_{hf} = \nu_{zf}\ /^{53}\gamma \quad \text{(Eq. 5)}$$

where $^{53}\gamma$ is the gyromagnetic ratio of the ^{53}Cr nucleus (in units of MHz/T). At 0 K, $\nu_{zf}(0)$ is related to the local magnetic moment at 0 K, M(0). The high field approximation is made here because the local field is the dominant determinant of the observed frequency. Other interactions can make small perturbations to the zero field frequency position [39]. The ground state magnetic moment M can be estimated from the spin-only contribution from the number, *n*, of unpaired electrons, $M = \sqrt{n(n+2)}$ or estimated as the average magnetic moment through the Landé g-factor for the ion ground state with

$$M = g\mu_B S \quad \text{(Eq. 6)}$$

where S = *n*/2 is the spin, and μ_B is the Bohr magneton per Cr ion (μ_B/Cr), and M can be directly measured using neutron diffraction or magnetometry. The ^{53}Cr Landé g-factor for ground state ions can be estimated from electron spin resonance measurements within ~ 4 % as 2 [40]. NMR measurements as the temperature approaches 0 K (liquid helium temperatures) in zero field are necessary to minimize thermal effects on the value of the hyperfine constants derived from the data and for comparison with quantum chemical calculations of hyperfine interactions. The sublattice magnetization and ν_{zf} will decrease as the temperature rises due to thermally excited spin waves. The relationship between the ^{53}Cr ν_{zf} near 0 K and the magnetic moment M near 0 K in μ_B per Cr ion can be described by

$$\nu_{zf}(0) = {}^{53}\gamma\,|A|\,M(0) \qquad \text{(Eq. 7)}$$

where |A| is the absolute value of the hyperfine coupling constant in T/μ_B. The gyromagnetic ratio of the ^{53}Cr nucleus, $^{53}\gamma$ = 2.406 MHz/T, is a constant. The absolute value of the hyperfine coupling constant, |A|, depends on the configuration and valence of the Cr ion in the compound, which is discussed in Section 4.7.1.

4.2 $(NH_4)_2CrO_4$ and $BaCrO_4$

Alkali metal chromates and alkaline-earth metal chromates have four Cr-O bonds of nearly equal length giving slightly distorted tetrahedral coordination of the Cr in the oxochromate (VI) anions, CrO_4^{2-}. This configuration restricts the magnitude of the efg at the Cr site, such that the coupling constant for the electric hyperfine interaction, C_Q, at the Cr site is typically less than 10 MHz [22]. In this circumstance the electric hyperfine interaction can be conveniently measured by conventional high applied field ^{53}Cr NMR via a simulation of a second-order perturbed lineshape [39] which yields C_Q and η (Eq. 2) where η measures the departure from axial symmetry of the efg tensor [29]. Ammonium chromate $(NH_4)_2CrO_4$ is monoclinic with space group *C2/m*, [41] whilst barium chromate $BaCrO_4$ is orthorhombic with space group *Pnma* [42]; both compounds have no electronic magnetic moment and no magnetic ordering.

Sharply defined ^{53}Cr NMR spectra are presented for $(NH_4)_2CrO_4$ and $BaCrO_4$ obtained at 9.4 T, along with DMFIT [43] simulations of the central transition based on second-order quadrupole perturbation theory, in **Figure 1**. The ^{53}Cr spectrum for $(NH_4)_2CrO_4$ has not been previously reported although a preliminary value for C_Q of ~2.5 MHz was mentioned in earlier work [44]. The values obtained here for C_Q and η in $BaCrO_4$ are in excellent agreement with parameters reported at higher fields as shown in **Table 1**. In these crystalline diamagnetic compounds, the central (1/2, –1/2) ^{53}Cr NMR transition displays relatively sharp singularities enabling accurate measurement of C_Q, η, and isotropic chemical shift δ_{iso} from the second-order quadrupolar features. The resulting isotropic chemical shift δ_{iso} = 0 ppm for both chromates, with the reference zero shift obtained from $(NH_4)_2CrO_4$ in aqueous solution, is in good agreement with the previously reported value of δ_{iso} = 1750±20 ppm for $BaCrO_4$ powder determined under MAS and referenced to $Cr(CO)_6$ in chloroform solution known to be shifted –1797 ppm relative to the CrO_4^{2-} used here [44,45]. Buhl [45] has calculated the chemical shift for CrO_4^{2-} using two density functionals and has reported values of 21 ppm and 81 ppm as compared to the experimental value of 0 ppm.

Table 1 ^{53}Cr quadrupolar coupling constant C_Q and asymmetry parameter η for $(NH_4)_2CrO_4$ and $BaCrO_4$ measured at 9.4 T compared with values previously reported.

Compound	**C_Q (MHz)**	**η**	**Field Strength (T)**	**Reference**
$(NH_4)_2CrO_4$	3.1±0.1	0.58±0.05	9.4	present work
$(NH_4)_2CrO_4$	~2.5	not reported	7.05 or 9.4	[44]
$BaCrO_4$	4.9±0.1	0.16±0.05	9.4	present work
$BaCrO_4$	5.0±0.05	0.14±0.03	11.75 and 18.8	[22]

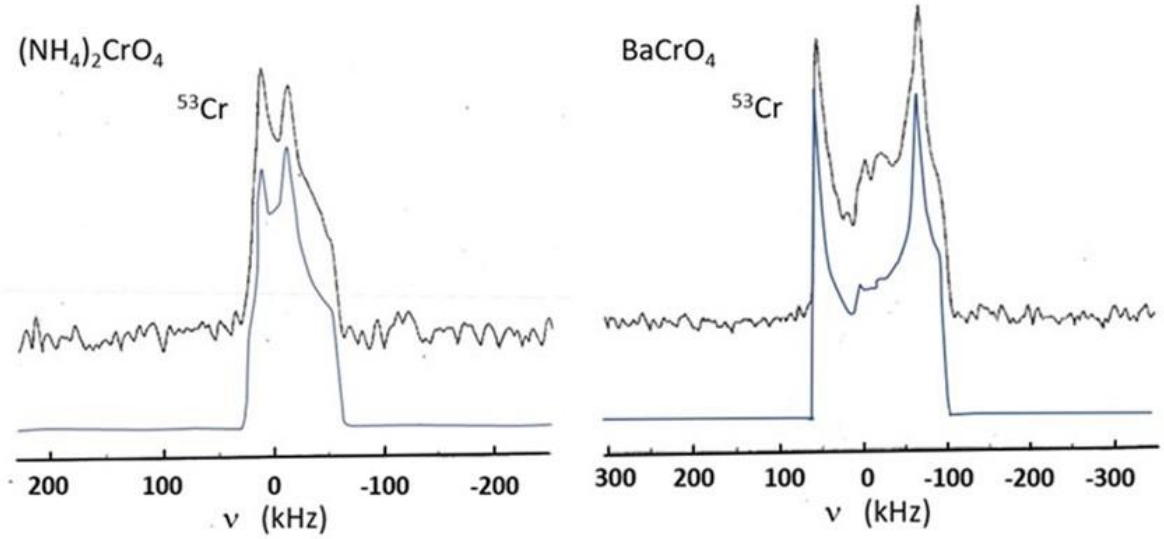

Figure 1. Experimental (top) and simulated (bottom) central (1/2, −1/2) transition static ^{53}Cr NMR lineshapes for static powder samples of $(NH_4)_2CrO_4$ (left) and $BaCrO_4$ (right) at 9.4 T. Intensity values are shifted on the y axis for clarity.

4.3 Cr_2N

Cr_2N is an interstitial compound showing metallic behavior and no magnetic transitions; its principal use is as a tempering agent in steel making. The crystal structure is trigonal [46] with a single Cr site (fully occupied) with no axis of symmetry. The powder XRD pattern [35] indicates a well crystallized specimen with minor impurity phases of $CrN_{0.98}$ (6±1%) and Cr (1.6±0.9%). It may be noted in passing that mono-chromium nitride, CrN, is an insulator at room temperature and an antiferromagnetic metal below the Néel temperature of 286 K [47]. *Ab initio* DFT calculations for two dimensional Cr_2N MXene have predicted an antiferromagnetic metal [48].

The ^{53}Cr and ^{14}N NMR spectra for Cr_2N are reported here for the first time. There exists a relatively substantial electric quadrupole interaction at the Cr site. The ^{53}Cr NMR spectrum (**Figure 2(a)**) at a magnetic field of 9.4 T has a width of approximately 300 kHz and a Knight shift of −1900 ppm. It was not possible to capture the spectrum using standard (echo) pulsed

NMR at a single operating frequency. The strategy employed here, and subsequently for the Cr_2O_3, was to record the amplitude using a frequency-stepped echo approach [32]. Simulation of the spectrum using DMFIT [43] gives C_Q = 6.3±0.2 MHz and η = 0.15±0.10.

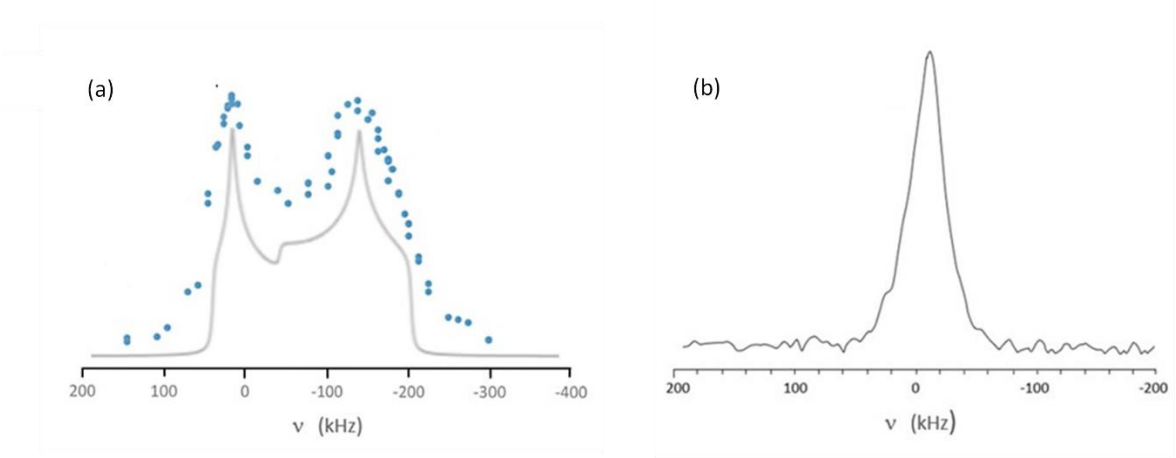

Figure 2. (a) Static ^{53}Cr NMR data from Cr_2N showing experimental (top) and simulated (bottom) central (1/2, −1/2) transition lineshape. Intensity values are shifted on the y axis for clarity. (b) Static ^{14}N NMR spectrum of Cr_2N.

The crystal structure [46] also indicates four N sites – one unoccupied, one fully occupied, and two partially occupied; however, a static pulsed ^{14}N NMR spectrum (**Figure 2(b)**) of the specimen indicates a single line with 35 kHz width (fwhm) and a small negative shift δ_{iso} = −200 ppm. The single narrow ^{14}N NMR line is somewhat surprising considering (i) the site symmetry of all the N sites is no higher than $\bar{3}$, and (ii) ^{14}N (I=1) is one of few quadrupolar nuclei with integer spin, and in non-cubic environments exhibits a first-order broadened ^{14}N NMR lineshape [39]. The observed line possibly originates from the one fully occupied site. This single line may be due to vacancy assisted mobility of the nitrogen atoms meaning that only the permanently filled site will be detected. Low temperature NMR measurements may shed light on the origin of the ^{14}N lineshape and are suggested as future work. From our room temperature lineshape, an upper limit value of C_Q < 0.047 MHz can be estimated from the fwhm [49]. Bastow *et al.* [50] have previously reported ^{14}N C_Q values for other metal nitrides including AlN (C_Q < 0.01 MHz). For AlN the ^{14}N static spectrum was an approximately Gaussian lineshape with fwhm of 7.5 kHz which gave the upper limit C_Q value ((4/3)fwhm) of < 0.01 MHz. This work has recently been revisited in a single crystal AlN specimen by Zeman *et al.* [51] reporting that C_Q = 8.19 kHz; hence this method is found to be robust for estimating an upper limit for C_Q within 20%.

4.4 CrB_2

The ^{53}Cr NMR lineshape for CrB_2 has not been previously reported. In the present work, frequency-stepped ^{53}Cr NMR was used to delineate the lineshape for CrB_2 at 295 K: a single, narrowly peaked, somewhat asymmetric lineshape (fwhm = 38 kHz) (**Figure 3(a)**) exhibiting a very large negative Knight shift: K_{iso} = –9982 ppm (–226 kHz at 9.4T). There is no second-order quadrupolar structure with distinct singularities of the central transition, suggesting a relatively small C_Q. However attributing the observed, relatively narrow, ^{53}Cr linewidth to

residual second-order quadrupolar broadening (Eq. 3), with I=3/2 and the Larmor frequency ν_L = 22.66 MHz at 9.4 T, yields an estimate for $\nu_Q \approx 1.285$ MHz giving $C_Q \approx 2.6 \pm 0.5$ MHz. This C_Q value for ^{53}Cr compares reasonably well with the value of 3.05 MHz calculated *ab initio* by Schwarz *et al*. [55]. There is some broader underlying intensity observed which probably comes from the satellite transitions given this small C_Q. The absence of a large quadrupolar interaction for ^{53}Cr is somewhat unexpected given the substantial nuclear quadrupole interaction exhibited at the metal sites by the isostructural neighboring group III and IV transition metal diborides ScB_2, TiB_2, and ZrB_2 [36], but the small C_Q estimated here for $^{53}CrB_2$ is consistent with the *ab initio* calculation [55]. These other diborides have sharp features for the second-order perturbed central transition splitting at the metal site, and the first-order perturbed satellite singularities can also be readily observed allowing precise determination of C_Q values, significantly different from what is observed here for CrB_2.

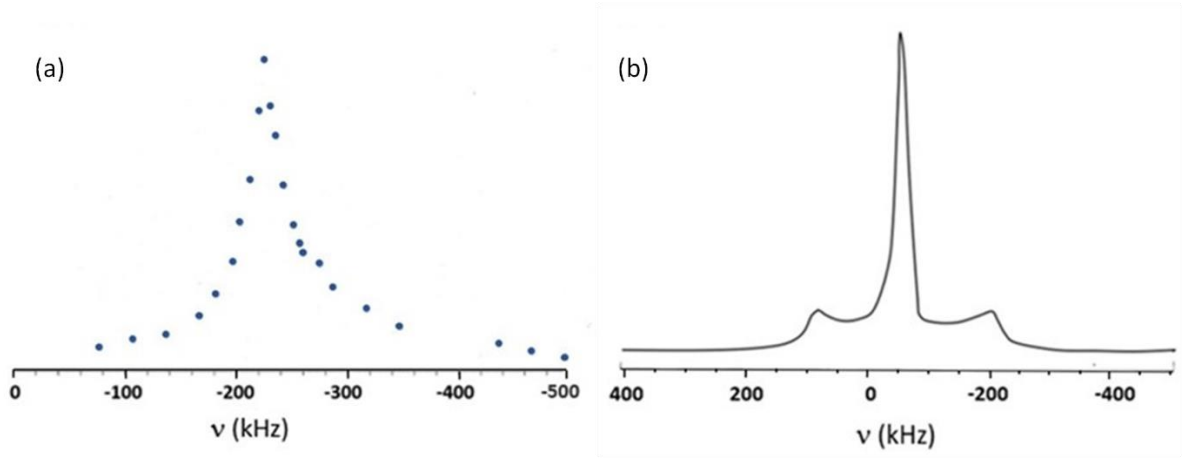

Figure 3. Static NMR data from CrB_2 showing (a) the central (1/2, −1/2) transition for ^{53}Cr and (b) the central as well as first-order quadrupole broadened (±3/2, ±1/2) transition for ^{11}B.

The $^{53}CrB_2$ lineshape has presumably gone undetected for decades due to the large negative Knight shift making it difficult to know where to search for the resonance. The Knight shift for pure Cr metal is large and positive, 6870 ppm [4]. Although the transition metal monoborides and diborides formed the basis of substantial early work, the ^{53}Cr resonance proved difficult to detect [56,57]. The present work may encourage ^{53}Cr NMR study of the bonding and electronic structure in the stable chromium borides, e.g. Cr_2B, Cr_5B_3, CrB, Cr_3B_4, CrB_4 and CrB_2 for comparison with theoretical predictions [58].

The ^{11}B NMR spectrum at 295 K exhibits a first-order quadrupolar lineshape [59]. For ^{11}B (I=3/2), the separation of the satellite transitions (±1/2, ±3/2) defines the quadrupolar frequency ν_Q (Eq. 3). For crystallographic sites with axial symmetry this equation simplifies as $\eta = 0$, and for ^{11}B (I=3/2) therefore $2\nu_Q = C_Q$. An ^{11}B NMR spectrum at 295 K yielding a C_Q of 0.58 MHz was measured as shown in **Figure 3(b)**. Schwarz *et al.* [55] calculated ^{11}B C_Q = 0.589 MHz in excellent agreement with this experimental value. The measured values of ^{11}B C_Q = 0.58 MHz and Knight shift = –390 ppm are in reasonable agreement with values first reported by Silver and Kushida [60] measured using continuous wave spectroscopy. The main ^{11}B lineshape was reported to vanish below 88 K [61] and a transition to

antiferromagnetism deduced. Subsequently Funahashi *et al.* [62], using neutron diffraction, observed a helical magnetic structure in CrB_2 below 88 K. Bauer *et al.* [53] confirmed the incommensurate spin order reported by Funahashi *et al.* [62]. Recent *ab initio* calculations for two dimensional CrB_2 have predicted a ferromagnetic half metal with T_C=175K [63].

4.5 CrO_2

In this ferromagnetic oxide the hyperfine interaction at the Cr site is sufficiently large that the ^{53}Cr spectrum can be conveniently examined in zero applied field. This interaction is progressively thermally averaged to lower values as the temperature rises from 4.2 K to the Curie temperature T_C = 395 K [17,64]. CrO_2 has the tetragonal rutile structure and is ferromagnetic below T_C. Until recently this compound was used as the magnetic coating for high quality magnetic tapes, and having a convenient Curie temperature relative to room temperature makes it attractive for use in flexible magnetic composite devices [64]. An SEM micrograph of the powder [35] displays a characteristic nanorod microstructure [19,20] with typical rod dimensions: length ~ 200 to 300 nm, diameter ~ 30 nm. The powder XRD pattern [35] indicates a well crystallized material with CrO(OH) (Guyanaite) detected as a minor impurity.

The rutile structure implies one distinguishable Cr site per unit cell, so that there should be only one central line visible in the ^{53}Cr zero field NMR spectrum. However two widely separated narrow lines of approximately equal intensity at frequencies ν_{low} and ν_{high} of 26.5 and 37.2 MHz, respectively, are observed at 4.2 K [16-18,20,21]. A self-doping mechanism has been tentatively suggested for the existence of two distinct Cr sites [17]. A hypothesis that the sites originate from intra-domain and domain wall Cr atoms, respectively, has been considered and experimentally discounted [17]. Recently, it has been hypothesized that the two different Cr sites have different 3d orbital occupation numbers [20]. Because CrO_2 is a half metal with a Curie temperature above ambient temperature, it is being investigated for use in spintronic devices [65].

The frequencies, ν_{low} and ν_{high}, for these two lines measured in this work at 77, 195 and 295 K (**Table 2**) were located by systematically searching frequencies below the reported values at 4.2 K. Increasing spin wave excitation as the temperature rises is presumably responsible for the steadily decreasing $\nu_{zf}(T)$ for the two Cr sites as the temperature rises (**Figure 4**). There is a correlation with Bloch ferromagnetic spin wave theory [9,11] that predicts a $T^{3/2}$ decrease in magnetization. Using Bloch theory, the data in **Figure 4** for the two Cr sites predict resonance frequencies at 0 K of 26.407 MHz and 37.068 MHz, indicating hyperfine fields at the nuclei of 12.7 and 17.8 T, respectively. The relationship between the hyperfine parameters, the magnetic moment and the chromium valence is further discussed in Section 4.7, as is spin wave theory.

The ^{53}Cr NMR linewidths diminish along with decreasing signal-to-noise ratio as the temperature rises towards the Curie temperature (**Table 2 and Figure 5**). Within experimental error, the frequency difference, ($\nu_{high} - \nu_{low}$), remains essentially constant as the temperature rises from 4.2 K with an average value of 10.55 MHz. Shim *et al.* [17] have reported the saturation magnetization (measured using a magnetometer) in CrO_2 from 10 to 380 K indicating a $T^{3/2}$ decrease in magnetization by 50% up to approximately 375 K, followed by a rapid continuous decrease of the remaining 50% of the magnetization toward zero in the critical region at the Curie temperature of 395 K. Recently, Piskunov *et al.* [21]

have measured ^{53}Cr NMR data from 4.2 K to 365 K in high purity CrO_2, giving values similar to those reported here.

It may be noted that there is no evidence of a quadrupole interaction in the $^{53}CrO_2$ NMR spectrum in the published or present data. Compare TiO_2 (also rutile structure) where the ^{49}Ti nuclei see a substantial efg (C_Q = 13.9 MHz, η = 0.19) [66] and α–VO_2 (rutile) where the ^{51}V C_Q = 2.77 MHz and η = 0.86. [67]. It is possible that the broad ^{53}Cr lines have a second-order quadrupole interaction folded in, which, since this quantity generally decreases with increasing temperature, would explain why the observed line widths decrease with increasing temperature. Takeda *et al.* [20] report single crystal $^{53}CrO_2$ NMR measurements at 4.2 K, in an applied magnetic field of 0.3 T parallel to the c axis, giving fwhm for the low and high resonances as 190 kHz and 280 kHz, respectively. A rough estimate of the upper limit for C_Q can be made from the narrowest linewidth that still obscures the quadrupolar splitting, where assuming η = 0 and perturbation theory still holds, a second-order perturbed quadrupolar linewidth Δ from Eq. 3 where I = 3/2, ν_L = 0.723 MHz at 0.3 T, then using the measured fwhm 190 kHz as Δ yields estimates for $\nu_Q \approx 0.513$ MHz and $C_Q \approx 1.03$ MHz. Our estimate of 0.513 MHz for ν_Q is in good agreement with a recent estimate of $\nu_Q \approx 0.5$ MHz [21]. It can be noted that a (hypothetical) value of η = 0.4 decreases C_Q by only 2.6%. To the best of our knowledge *ab initio* calculations of the ^{53}Cr efg in CrO_2 have not been published.

Table 2 CrO_2 ^{53}Cr zero field NMR line peak frequencies ν_{high} and ν_{low} and linewidths $\Delta\nu$ at various temperatures below T_C.

T(K)	$T^{3/2}$ ($K^{3/2}$)	ν_{low} (MHz)	$\Delta\nu$ (kHz)	ν_{high} (MHz)	$\Delta\nu$ (kHz)	Reference
4.2	8.6	26.5	450	37.2	680	[20]
6.5	16.6	26.4	485	37.1	450	[17]
77	676	25.3	530	35.9	510	present work
195	2723	23.3	510	33.7	460	present work
295	5067	20.2	390	30.7	420	present work

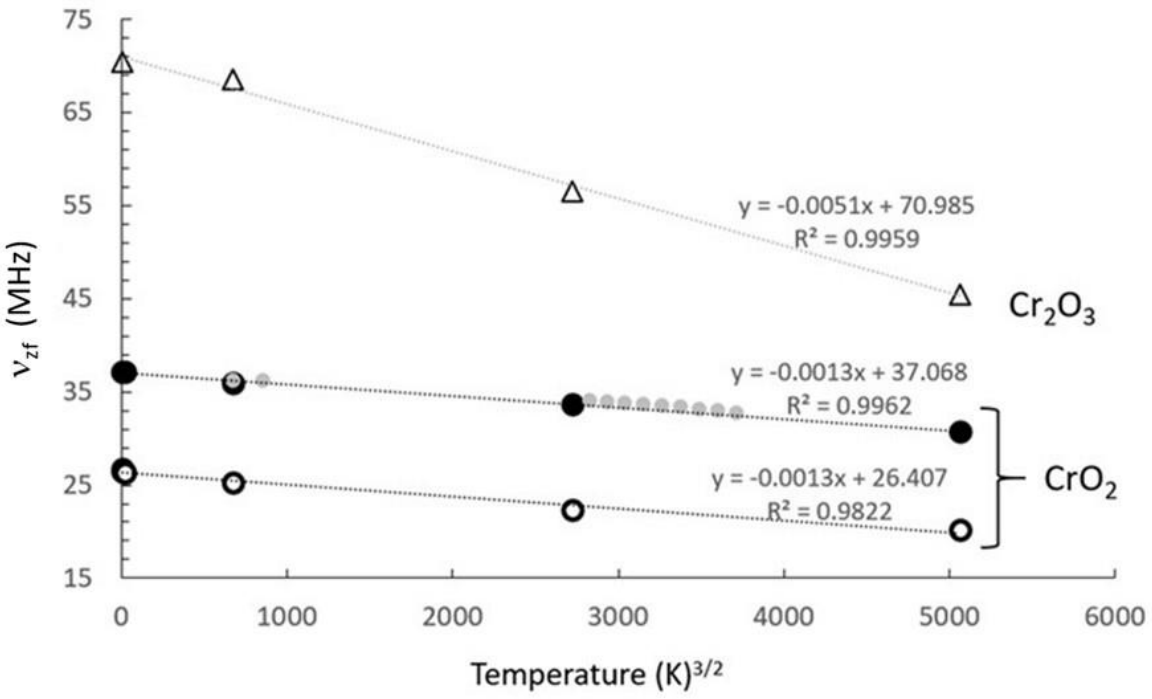

Figure 4. ^{53}Cr frequencies ν_{high} (●) and ν_{low} (**O**) for CrO_2 plotted as a function of $T^{3/2}$. With best fit equation and R^2 value displayed for the dotted line fits. Data of Yasuoka *et al.* [15] for $^{53}CrO_2$ ν_{high} (●) included for information as described in the text. ^{53}Cr frequency (Δ) for Cr_2O_3 plotted as a function of $T^{3/2}$ with best fit displayed.

The resonance reported by Yasuoka *et al.* [15] in 1963 for CrO_2 was detected using a marginal oscillator and a super-regenerative oscillator. The resonance, which can be attributed to ν_{high}, was reported for eleven temperatures over a range from 77 to 240K. These data were added to the data shown in **Figure 4** in order to further refine the fit to spin wave theory $T^{3/2}$ and resulted in a best fit, $y = -0.0012x + 37.104$ ($R^2 = 0.9866$), in excellent agreement with that obtained from frequencies measured using zero field pulsed NMR. It can be noted that neither a T^2 fit nor a linear T fit to these data was as good as the $T^{3/2}$ fit [11]. Comparison of the ^{53}Cr zero applied field NMR frequency, ν_{high}, from the present work, Yasuoka *et al.* [15], and Piskunov *et al.* [21], with the saturation magnetization data of Shim *et al.* [17] as functions of temperature for CrO_2, show agreement with Bloch spin wave theory to T = 340 K or $T = 0.86T_C$ [35]. Data from 340 K to 365 K (up to $0.9T_C$) indicate a rapid continuous decrease of ν_{high} and ν_{low} toward zero in the critical region near the Curie temperature of 395 K [21] although the values of ν_{zf} are still at the 40-50% level of decrease from 4.2 K when measured at 365 K [35]. It remains to be demonstrated whether the local ^{53}Cr sublattice magnetization transition at T_C = 395 K is first-order, i.e. a discontinuous drop to zero of spontaneous magnetization (rather than a smooth transition to the paramagnetic state; i.e. zero magnetization). ^{53}Cr NMR measurements up to and through T_C (395 K) are suggested for future work.

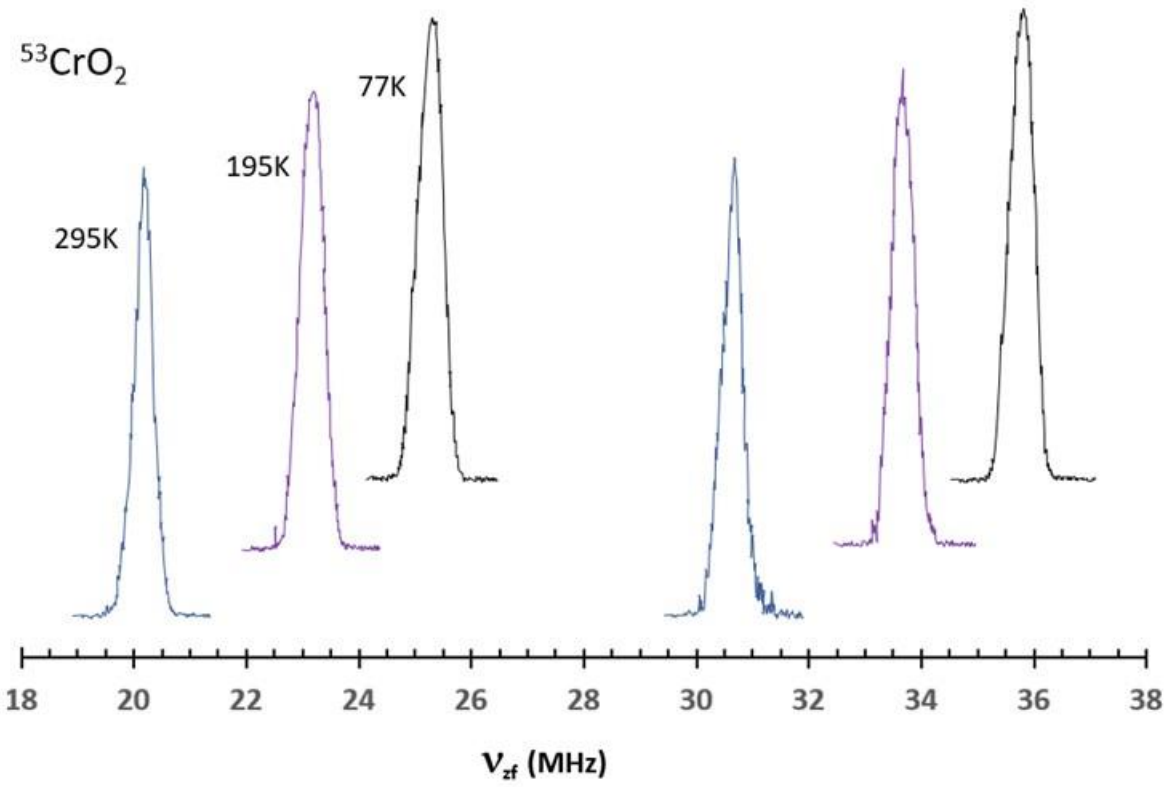

Figure 5. ^{53}Cr NMR lineshapes for CrO_2 at 295, 195 and 77 K. Intensity values are shifted on the y axis for clarity.

4.6 Cr_2O_3

This antiferromagnetic compound has the corundum (Al_2O_3) structure with one distinguishable Cr atom per unit cell at a site with axial symmetry so that any detectable second-order lineshape should indicate an efg with $\eta = 0$. An XRD pattern [35] indicated good crystallinity with no trace of impurity. The antiferromagnetic to paramagnetic transition temperature, Néel temperature, T_N = 307.9 ± 0.2 K, was measured using DSC. The DSC traces were made on two separate samples of the powder, and both measurements [35] indicate a lambda anomaly in specific heat at T_N, characteristic of a second-order phase transition.

Antiferromagnetic ordering was established in Cr_2O_3 by Brockhouse in 1953 [68] and Corliss *et al.* [69,70]. Previous internal NMR, as discussed in Section 2, has been reported by Rubinstein *et al.* [14] using a super-regenerative oscillator detector, with a ^{53}Cr 95% enriched specimen at temperatures from 1.6 to 16 K. Over this relatively small temperature range the NMR line was detected at a constant frequency of 70.43 MHz, with the signal disappearing into the noise above 16 K. The frequency separation of the satellites (^{53}Cr, I=3/2) gave ν_Q = 0.525 MHz and C_Q = 1.05 MHz using Eq. 4 for η=0. Takeda *et al.* [19] using a much later, spectroscopically more sophisticated, method, recently reported a similar value of ν_Q = 0.54 MHz. The ^{53}Cr NMR spectrum of Takeda *et al.* [19] at 4.2 K is reproduced here in **Figure 6**; its sharp central line centered at 70.43 MHz with clear (±1/2, ±3/2) satellites measuring ν_Q = 0.54 MHz (C_Q = 1.08 MHz) can be compared with the ^{53}Cr spectra reported in the present work as described below.

In the present work, the ^{53}Cr zero field NMR signal was searched for below 70.43 MHz, first at 77 K. This search revealed a surprisingly broad lineshape (**Figure 6)** centered at 68.5 MHz with width 1.7 MHz, delineated by frequency stepping. A search at 195 K located, again by frequency stepping, a somewhat broader essentially featureless lineshape of width 2.0 MHz centered at 56.5 MHz. At 295 K a single line at 45.5 MHz of fwhm = 0.16 MHz was measured. The 295 K measurement was repeated and verified the original result. Spectra taken at increasing positive and negative 50 kHz frequency offsets from this value confirmed a single absorption line at 45.5 MHz. It is unclear what line broadening mechanism is operating at 77 and 195 K and what is happening to remove this mechanism at 295 K. The specimen was studied over a wide temperature range (10-300 K) using synchrotron radiation powder XRD, and there was no indication of a phase transition. The DSC trace [35] starts upwards from 140 K and there are no transitions other than the Néel temperature at 307.9 K. Karnachev [71] studied the rare earth orthochromite $Dy_{0.2}Er_{0.8}CrO_3$ (T_N = 141K) over the temperature range 58-91 K using zero applied field NMR and observed line broadening attributed to efg inhomogeneity. We can find no other report of line broadening in Cr_2O_3 and suggest further exploration of the mechanism as potentially fruitful future experimental work and DFT calculation. **Figure 4** shows a plot of the central line frequency for ^{53}Cr in Cr_2O_3 as a function of $T^{3/2}$ consistent with spin wave theory, predicting a resonance frequency at 0 K of 70.985 MHz, indicating a hyperfine field at the nucleus of 34.1 T. A hyperfine magnetic field of approximately 19 T still exists at approximately 10 K below the Néel temperature (**Figure 4**). Corliss *et al.* [69,70] showed that greater than 50% of the macroscopic magnetization decrease in Cr_2O_3 powder (measured using neutron diffraction) occurs in the critical region between 295 K and the Néel temperature [35]. The present work suggests that ^{53}Cr studies of the magnetic sublattice in Cr_2O_3 over a wide temperature range inclusive of T_N will be fruitful.

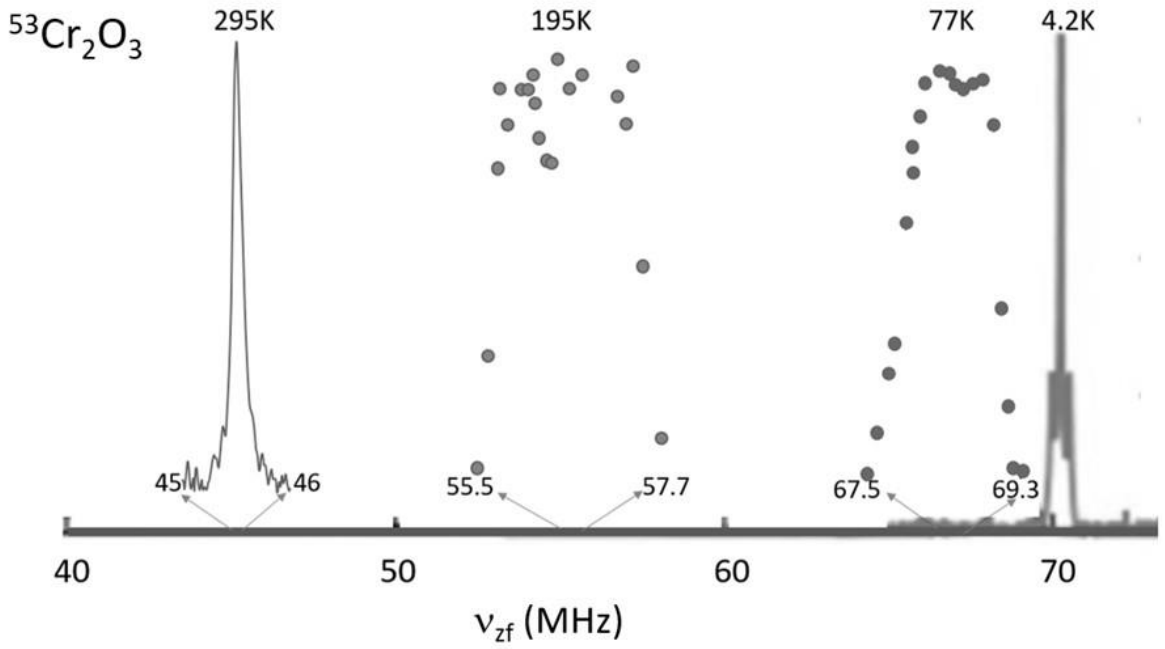

Figure 6. ^{53}Cr NMR lineshapes for Cr_2O_3 in zero field over a range of temperatures. Spectrum at 4.2 K adapted from Takeda *et al.* [19].

4.7 Compilation of ^{53}Cr solid-state NMR in alloys and compounds

Chromium exhibits seven valence states in its alloys and compounds with the most prevalent being Cr(0) for the metal, metallic alloys, and strong field ligand complexes, and Cr(III) and Cr(VI) for other compounds. The present work has reported NMR spectra for $3d^6$ Cr(0) paramagnetic (Cr_2N) and $3d^6$ Cr(0) antiferromagnetic (CrB_2) metals, a $3d^3$ Cr(III) antiferromagnetic (Cr_2O_3) semiconductor, a $3d^2$ Cr(IV) ferromagnetic half metal (CrO_2), and $3d^0$ Cr(VI) diamagnetic ($BaCrO_4$, $(NH_4)_2CrO_4$) insulators. As discussed, ^{53}Cr magnetic resonance data can be used to elucidate the bonding environment of Cr in materials. **Table 3** summarizes the calculated integer valence and theoretical spin-only magnetic moments expected for chromium in its compounds as compared to the range of reported low temperature measured magnetic moments [72-76]. **Table 4** comprehensively summarizes ^{53}Cr magnetic resonance data for the compounds reported here within the context of data from the literature on Cr alloys and compounds [77-117]. To the best of our knowledge, past ^{53}Cr solid-state NMR studies have not been tabulated in one place since 1971 [118]. For the literature surveyed here, which covers 1961 to 2022, 73% of the compounds studied are magnetic compounds, with 27% of those having their critical magnetic ordering temperature (T_C or T_N) above 300 K. For these studies of magnetic materials, 89% report NMR data at zero applied magnetic field.

4.7.1 Zero applied field NMR at low temperatures

This section will first focus on magnetic ^{53}Cr compounds and their NMR data at zero applied magnetic field. In **Table 4**, for zero applied field NMR reports, we include the low temperature resonance position of the central line(s); in reports where domain and wall resonances are distinguished, we have included only the data from domains; in reports where T_C or T_N > 77 K and measurements were made at both liquid helium and liquid nitrogen temperatures we have included those data for comparison purposes. For the spin echo technique, only domain signals are observed due to the short relaxation times of the broad resonance signals from walls. Three low temperature zero field NMR reports attribute separate resonances to domain and domain wall sites [3, 94, 119] for CrI_3, $EuCrO_3$, and $CrBr_3$, respectively, with the domain wall resonances located from 0.89 MHz to 1.42 MHz below the domain resonances. Where possible, low temperature Cr valence is given and it should be noted that in some compounds (mixed valence or those with a phase transition), valence can change with temperature.

The background to the hyperfine interactions at zero applied magnetic field, where the center-line resonance, ν_{zf}, (in units of MHz) is a measure of the hyperfine field at the ^{53}Cr nucleus, has been introduced in Section 4.1 (Eqs. 4 to 6) under the approximations noted above. NMR measurements as the temperature approaches 0 K (liquid helium temperatures) in zero field are necessary to minimize thermal effects on the value of the hyperfine constants derived from the data and for comparison with quantum chemical calculations of hyperfine interactions. The sublattice magnetization, and the resonance frequency, will decrease as the temperature rises due to thermally excited spin waves. ^{53}Cr zero applied field and magnetization measurements for CrO_2 and Cr_2O_3 [35] illustrate the frequency-magnetization relationship, i.e., proportionality of $\nu_{zf}(T)$ and M(T), along with the $T^{3/2}$ relationship for temperatures up to ~ 0.8 (T_C or T_N) (cf. **Figure 4**).

The absolute value of the hyperfine coupling constant |A| depends on the configuration and valence of the Cr ion in the compound, indicates the extent of delocalization of the unpaired electron, and can be calculated *ab initio* for the $3d^n4s^0$ ions [120] or calculated from the measured values of $\nu_{zf}(0)$ and M(0) for a given compound [1]. Several authors [120-122] calculate A for the chromium $3d^n4s^0$ ions, giving the core polarization hyperfine field per unpaired valence electron, within the Hartree-Fock scheme, as −12.5 T/μ_B. This value results from the approximation of (i) the magnetic hyperfine 3d exchange interaction transferred at the chromium nucleus (through covalency and overlap) as the Fermi contact interaction and (ii) the magnetic moment as the spin density at the nucleus. Values of A derived from low temperature experiment are compared with theory to ascertain the extent of delocalization or magnitude of the transferred field. Alternatively, theoretical values of A are used with measured values of ν_{zf} at low temperature to predict magnetization and valence. The ground state magnetization can also be calculated using *ab initio* DFT methods where the approximation of the exchange and correlation potential is the subject of much research in chromium compounds [123-126].

Other methods for the calculation of the hyperfine coupling constant have been reported for ^{53}Cr with values of |A| ranging from 8.3 to 12.2 T/μ_B [126-130]. The value A = −10 T/μ_B is often used, as this is the average value for the core polarization hyperfine field per unpaired valence electron for the 3d transition metals reported by Blugel *et al.* [129]. The value of |A| = 8.33 T/μ_B results from a first principles calculation of the contact field for Cr^{3+} [126]. Rubinstein *et al.* [14] first reported the measured value of A = –9.76 T/μ_B based on zero applied field measurements of $^{53}Cr^{3+}$ in an octahedral environment of oxygen atoms in Cr_2O_3 with ν_{zf} = 70.43 MHz at 1.6 K and with M(0) assumed to be 3 μ_B per Cr atom. The theoretical value of |A| for an isolated Cr^{3+} ion (12.5 T/μ_B) has been shown to be very close to the measured values (11.3 to 12.4 T/μ_B) in Cr molecular rings and chains [10,104,105]. The theoretical values compare favorably with the range of measured (calculated from measurements on Cr compounds) values of |A| shown in **Table 3**.

Table 3 is also useful for estimating the range of observed frequencies near 0 K for the ^{53}Cr nucleus in various compounds. Using the range of |A| values and the spin-only magnetic moment values, the anticipated range of ^{53}Cr $\nu_{zf}(0)$ is 38-110 MHz; using the measured local magnetic moment values, the anticipated range is 10-114 MHz; as compared to the reported measured range of ν_{zf} in **Table 4** which is 13-82 MHz. This measured range of $\nu_{zf}(0)$ reported for each configuration in **Table 4** can be compared to the range calculated from **Table 3** in a form of Slater-Pauling-like curve (see **Figure 7**). The Slater-Pauling curve (magnetic moment M as a function of valence electron concentration) for 3d transition metal compounds has been calculated *ab initio* by Dederlichs *et al.* [130] for Fe, Ni, and Co based alloys. Such an *ab initio* calculation for Cr-based alloys has not been reported and is recommended as fruitful future work.

The theoretical value |A| = 8.33 T/μ_B, [126] along with the spin-only magnetic moment values from **Table 3** for each valence, are used to calculate the theoretical internal field frequencies for each valence in **Figure 7 (b)**. **Figure 7 (b)** shows that the value of the hyperfine interaction constant |A| has a great bearing on the goodness of fit between theory and experiment. It can be noted that a variation in |A| from 8.3 to 12.5 T/μ_B results in a variation of predicted resonance frequency (e.g. for Cr(III), using spin-only M = 3 μ_B) from 60 to 90 MHz. In addition, it should be noted that in **Figure 7 (b)** the mixed valence compounds are shown together at the boundaries of the integer valence values, which may also affect goodness of fit.

Future work on *ab initio* calculations for magnetic Cr alloys and compounds would be useful and could help predict the mixed valence values for $\nu_{zf}(0)$. Mixed valence is thought to enable local double exchange mediated magnetic order [131] which, in topological insulators, is postulated as a pathway to room temperature quantum transport in zero magnetic field [132,133]. Also, *ab initio* calculations of $\nu_{zf}(0)$ would be helpful for locating Cr(I) and Cr(V) internal field resonances that, to the best of our knowledge, have not yet been reported by zero field NMR studies. In **Figure 7 (b)** we have indicated, with dashed line ellipses, where one might expect to find the low temperature ^{53}Cr zero applied field NMR resonances for $3d^5$ low spin and $3d^1$ compounds in future experiments or calculations.

Some further comments on **Figure 7 (b)** are warranted as it is the first time the literature data for ^{53}Cr have been compiled in such a format. As reviewed in this section, previous ^{53}Cr reports have mainly focussed on a single material with a single Cr valence (predominantly Cr^{3+}), with authors choosing either to fix the hyperfine coupling constant A or to fix the magnetic moment. The data in **Figure 7 (b)** now provide a summary of ^{53}Cr $\nu_{zf}(0)$ values for a wide range of Cr compounds across the valences Cr(0) to Cr(IV) including mixed valence, high spin, low spin, octahedral and tetrahedral configurations, metals, half metals, semiconductors, insulators, and varying crystal and magnetic structures. These data allow us to test our understanding of magnetism in Cr alloys and compounds. Cottenier [134] has noted the difficulty of DFT functionals in capturing the physics of the ground state for Cr alloys and compounds, making these alloys ideal testing grounds for improved DFT functionals. The data set may also prove helpful as a training set for a machine learning approach to property prediction as well as testing hypotheses and models.

1. It can be found in the literature that the covalency of the Cr-x bond increases as x=O is successively replaced by x=halides, x=S, and x=Se [121]. The "covalency school model" [121] expects the magnetic moment of the electron spins (and hence ν_{zf}) to decrease with decreasing electronegativity, i.e. with increasing covalency, which it does as shown in **Figure 7 (b)** for d^3 $Cr(III)^{oct}$ oxides, halides, sulfides and selenides.
2. The reported non-integer valence values for mixed valence compounds from **Table 4** have been plotted as an expanded section [35] and show the expected decrease in low temperature ^{53}Cr internal magnetic field resonance frequency with valence from Cr^{3+} to Cr^{4+} for mixed valence chromium oxides.
3. The two Cr^{2+} high spin d^4 $Cr(II)^{oct}$ compounds may appear as outliers; however, they are high spin and sit approximately where they would be predicted using the spin-only magnetic moment M = 4 and $|A| = 8.33$ T/μ_B.

Table 3. Magnetic moment, integer valence, and ionic radius of chromium in its alloys and compounds.

Configuration	**Valence**	**Number of unpaired electrons, *n*** **Spin S=*n*/2**	**Spin-only Magnetic moment, M (μ_B) calc** **M=$\sqrt{n(n+2)}$**	**Magnetic moment, M (μ_B) measured** [72] **Octahedral | Tetrahedral**		**Average Magnetic Moment, M (μ_B)** **M = gμ_BS** **(using g=2)**	**Hyperfine Coupling Constant** |A| **(T/μ_B)**	**Metallic or Ionic Radius (pm)** [73,74]	**Cr Valence Reference Standard Compounds** [75,76]
Cr (0) $[Ar]3d^5 4s^1$ configuration is for a non-bonded isolated Cr	Cr	6 S=3	6.93	NA	NA	6	Theory 12.5	140	NA
Cr (0) $[Ar]3d^6 4s^0$	Cr	hs 4 ls 0 S=2 S=0	4.90 0	ls 0.4-0.6		4 0	Measured 11.3-13.9	ls 128	Cr, $Cr(CO)_6$
Cr (I) $[Ar]3d^5 4s^0$	Cr^+	hs 5 ls 1 S=$\frac{5}{2}$ S=$\frac{1}{2}$	5.92 1.73	ls 1.77		5 1	9.8	ls 109	$(C_6H_6)_2CrI$
Cr (II) $[Ar]3d^4$	Cr^{2+}	hs 4 ls 2 S=2 S=1	4.90 2.83	hs 4.0-5.0 ls 2.7-3.4		4 2	8.6 7.5-9.0	hs 80 ls 73	CrSe $CrCl_2$
Cr (III) $[Ar]3d^3$	Cr^{3+}	3 S=$\frac{3}{2}$	3.87	2.7-4.0		3	9.0-12.7	61.5	$CrCl_3$, Cr_2O_3
Cr (IV) $[Ar]3d^2$	Cr^{4+}	2 S=1	2.83		2.6-2.8	2	5.6-8.0	55	CrO_2
Cr (V) $[Ar]3d^1$	Cr^{5+}	1 S=$\frac{1}{2}$	1.73		1.7-1.8	1	7.4-7.8	49	$CrOCl_3$, $YbCrO_4$, $NdCrO_4$
Cr (VI) $[Ar]3d^0$	Cr^{6+}	0 S=0	0		0	0	NA	44	CrO_3, $CaCrO_4$, K_2CrO_4, $K_2Cr_2O_7$

hs=high spin, ls=low spin. The notation Cr (I, II, …) for oxidation state should not be confused with some authors' use of this nomenclature for inequivalent Cr atom positions in a unit cell.

Table 4. ^{53}Cr hyperfine interaction parameters of chromium compounds from magnetic resonance measurements. Cr valence expected at 0 K. Local magnetic moment near 0 K, when reported. Note the measurement temperature, because the chemical shift δ_{iso} or Knight shift for metals, the zero applied field NMR center line frequency, the Cr sublattice magnetization, and the Cr ion valence can be functions of temperature. Material character and critical magnetic transition temperatures are given where known.

Compound	**Chromium Valence** **Local Magnetic Moment**	**δ_{iso} or Knight shift (ppm)***	**Center line frequency (MHz)**	**C_Q (MHz)**	**η**	**Temperature (K)** **AFM =** antiferromagnetic **FM =** ferromagnetic **PM =** paramagnetic	**Character**	**Reference**
Cr	Cr(0) 0.5μ_B/Cr	6870	16.60			314 to 387 314	Metallic, AFM below T_N = 313K, PM above	[4] [31]
$Cr_{1-x}V_x$ (x = 0.25 to 3 at%)	Cr(0)	6850 to 6990				300	Metallic, AFM below T_N = 287K (0.25 at% V) to 65K (3 at% V), PM above	[4,5]
$Fe_{1-x}Cr_x$ (x = 0.25 to 26.3 at%)	Cr(0) 0.46μ_B/Cr		15.85 to 17			1.2	Metallic, FM below T_C = 1050K (0.25 at% Cr) to 920K (26.3 at% Cr), PM above	[77]
$Cr_{1-x}Mo_x$ (x = 12.9 to 22.6 at%)	Cr(0)	6800				1.4	Metallic, AFM below T_N = 146K (12.9 at% Mo) to 20K (22.6 at% Mo), PM above	[28]
Cr_3AsN (2 inequivalent sites)	Cr(0) 0.5μ_B/Cr		13.66, 14.51		0 0	4 4	Metallic, itinerant AFM below T_N = 255K, PM above	[78]
$CrH_{0.93}$ and $CrH_{0.97}$ (hexagonal)	Cr(0)	5300				3 to 300	Metallic, paramagnetic	[27]

$CrH_{0.93}$ and $CrH_{0.97}$(cubic)	Cr(0)	3000				3 to 300	Metallic, paramagnetic	[27]
$Al_{1-x}Cr_x$ (x = 0.1 and 0.5 at%)	Cr(0)	–3800				1 to 4	Metallic, dilute substitutional site	[79]
$Pt_{1-x}Cr_x$ (x = 0.1 and 0.5 at%)	Cr(0)	–8200				1 to 4	Metallic, dilute substitutional site	[80]
CrB_2	Cr(0)	–9982		2.57[a]	0	295	Metallic, weak itinerant AFM below T_N = 88K, PM above	present work
Cr_2N	Cr(0)	–1900		6.3	0.15	295	Metallic, paramagnetic	present work
$Cr(CO)_6$	Cr(0)	–1814**		0.348	0.48	295	Insulator, diamagnetic	[44]
Rb_2CrCl_4	$Cr(II)^{oct}$ $4\mu_B$/Cr		82.3 67.4[b]	3.2		4.2	Semiconductor, FM below T_C = 52K, PM above	[81]
$SrCr_2As_2$	$Cr(II)^{oct}$ $1.9\mu_B$/Cr		71	[c]		1.6	Metallic, AFM below T_N = 615K, PM above	[82]
Cr_3Te_4 (2 inequivalent sites)	Cr(II), Cr(III) $1.79\mu_B$/Cr or $2.35\mu_B$/Cr		57.5, 45.3 56.0, 44.5 55.2, 44.8 50.0, 36.9 47.0, 36.5			4.2 4.2 20 77 77	Metallic, FM below T_C = 329K, PM above	[83] [84] [85] [84]
Cr_5Te_6 (2 inequivalent sites)	Cr(II), Cr(III) $2.5\mu_B$/Cr		53.0, 41.0			77	Metallic, FM below T_C = 327K, PM above	[84]
Cr_7Te_8 (2 inequivalent sites)	Cr(II), Cr(III) $1.8\mu_B$/Cr		58.2, 45.1 52.6, 40.8			4.2 77	Metallic, FM below T_C = 350K, PM above	[86]

CrTe (2 inequivalent sites)	Cr(II), Cr(III) 2.4μ_B/Cr		54.0, 42.2 55.2, 45.1			77 77	Metallic, FM below T_C = 340K, PM above	[85,87] [84]
$Y_3Fe_{4.57}Cr_{0.43}O_{12}$	Cr(III)		78.8 78.0			4.2 77	Insulator, ferrimagnetic below T_C = 500K, PM above	[88]
$CrCl_3$	Cr(III) 2.9μ_B/Cr		62.42 62.32	0.882 0.9	0	1.23 1.4	Semiconductor, AFM below T_N = 16.8K, PM above	[2] [13]
$CrBr_3$	Cr(III) 2.99μ_B/Cr		58.038	1.184	0	1.34	Semiconductor, FM below T_C = 37K, PM above	[1]
CrI_3	Cr(III) 3.1μ_B/Cr		49.392	0.744	0	1.65	Semiconductor, FM below T_C = 68K, PM above	[3]
$CuCrO_2$	Cr(III) 2.8μ_B/Cr		63.8 to 66.0			4.2	Insulator, AFM below T_N = 24.3K, T_N = 23.6K, PM above	[89]
Cr_2O_3	Cr(III) 2.48μ_B/Cr		70.43 70.43 68.5	1.05 1.08	0	1.6 4.2 77	Semiconductor, AFM below T_N = 308K, PM above	[14] [19] Present work
$Dy_{0.2}Er_{0.8}CrO_3$	Cr(III)		63.6	4.4	0	69	Semiconductor, AFM below T_N = 141K, PM above	[71]
$GdCrO_3$ (2 magnetic sublattices)	Cr(III)		68.8 68.3	4.4 1.88	0	4 10	Insulator, AFM below T_N = 170K, PM above	[90]
$ErCrO_3$ (low T AFM phase, higher	Cr(III)		68.97 67.6	2.7 1.8	0 0	4.2 (AFM) 37 (weakly	Insulator, weakly FM below T_C = 133K, PM	[91] [92]

T weakly FM phase)						FM)	above	
$TmCrO_3$ (2 magnetic sublattices)	Cr(III)		68.9 69.1	1.36 3.52	0 0	1.8 to 5.6 1.8 to 65	Insulator, AFM below T_N = 125K, PM above	[93]
$LuCrO_3$	Cr(III)			2.92	0	4.2	Insulator, AFM below T_N = 120K, PM above	[94]
$EuCrO_3$	Cr(III)		68.7	2.76	0	14.3	Insulator, AFM below T_N = 140K, PM above	[94]
$LaCrO_3$	Cr(III)		68.63			4.2	Semiconductor, AFM below T_N = 290K, PM above	[95]
$MnCr_2O_4$	Cr(III)		66.5 66.2			4.5 6.5	Insulator, ferrimagnetic below T_C = 41K, PM above	[96] [97]
$CuCr_2O_4$	Cr(III)		63 63.2 59.4			5 0[d] 77	Insulator, ferrimagnetic below T_C = 135K, PM above	[98] [99]
$FeCr_2S_4$	Cr(III)		50.8 46.8			0 [d] 77	Metallic, ferrimagnetic below T_C = 180K, semiconductor PM above	[99]
$CoCr_2S_4$	Cr(III) 2.7μ_B/Cr		49.3 47.4			0 [d] 77	Semiconductor, ferrimagnetic below T_C = 222K, PM above	[87]
$Mn_xZn_{1-x}Cr_2O_4$ ($x \geq 0.7$)	Cr(III)		65.5			1.8	Insulator, ferrimagnetic below T_C = 41K, PM above	[100]
$Ga_{0.2}Fe_{0.8}NiCrO_4$	Cr(III)		75			4.2	Insulator, frustrated ferrimagnetic below T_C =	[101]

							480K, PM above	
$NaCrS_2$	Cr(III)		53.45	0.2		1.5	Semiconductor, AFM below T_N = 17K, PM above	[102]
Cr_3As_2	Cr(III)		56.0 55.8			77 81.4	Insulator, ferrimagnetic below T_C = 243K, PM above	[103]
Cr_7Ni	Cr(III)					1.6	Semiconductor, AFM ring	[104]
Cr_7Cd (3 inequivalent sites)	Cr(III)		(44, 46, 57)[b]			1.6	Semiconductor, AFM ring	[105]
Cr_8Cd	Cr(III)					1.6	Semiconductor, AFM ring	[8]
$YCrO_3$	Cr(III)		68.73 68.74	1.99 2.0 1.52	0 0 0	4.2 4.2 77	Insulator, AFM below T_N = 140K, PM above	[106] [19] [94]
$NaCr_2O_4$	Cr(III), Cr(IV): $Cr^{3.5+}$		52			4.2	Insulator, AFM below T_N = 125K, PM above	[107]
$K_2Cr_8O_{16}$ (4 inequivalent sites: A,B,C,D)	Cr(III), Cr(IV): $Cr^{3.75+}$ $2.25\mu_B$/Cr		A 46,56 B 46,56 C 43,53 D 39,49			4.2	Half metal, FM below T_C = 180K PM above, metal-insulator transition T_{MI} = 95K	[19]
$SrRu_{1-x}Cr_xO_3$ (x = 0.05, 0.12)	Cr(III), Cr(IV): $Cr^{3.75+}$ $2.4\mu_B$/Cr		60.8 (x = 0.05) 60.3 (x = 0.12)			1.3	Insulator, itinerant FM below T_C = 175 to 186K (x = 0.05, 0.12), PM above	[108]
$CuCr_2Te_4$	Cr(III), Cr(IV)		34.9			77	Semiconductor, FM below T_C = 326K, PM above	[109]

$CuCr_2Se_4$	Cr(III), Cr(IV)		38.2			77	Semiconductor, FM below T_C = 430K, PM above	[109] [110]
$ZnCr_2Se_4$	Cr(III), Cr(IV) or Cr(III) 1.9μ_B/Cr		46.7 44.75	1.48		1.4 6	Semiconductor, AFM below T_N = 20K, PM above	[111] [6]
$CuCr_2S_4$	Cr(III), Cr(IV) 2.67μ_B/Cr		39.8 38.9 27		0	4.2 77 300	Metallic, FM below T_C = 420K, semiconductor PM above	[112] [113]
$CuCr_{2-x}V_xS_4$ (x= 0.1, 0.25, 0.375)	Cr(III), Cr(IV)		30 to 55			4.2	Metallic, FM below T_C = 267K (for x=0.25), semiconductor PM above	[112]
$CuCr_{2-x}Sb_xS_4$ (x=0, 0.02, 0.07)	Cr(III), Cr(IV)		39.5 39.3 39.4	1.8 1.8 1.8	0 0.1 0.2	77 77 77	Metallic, FM below T_C = 420K, semiconductor PM above	[110]
$Cd_{1-x}Ag_xCr_2Se_4$ (x=0, 0.001, 0.005, 0.015)	Cr(III), Cr(IV)		44.05	3.68		4.2	Semiconductor, FM below T_C = 130K, semiconductor PM above	[114,115]
$CdCr_2Se_4$	Cr(III), Cr(IV)		44.06 34.8	3.52	0	4.2 77	Semiconductor, FM below T_C = 129K, PM above	[116] [109]
$CdCr_2S_4$	Cr(III), Cr(IV)		46.02 45.97	3.80	0	1.4 4.2	Insulator, FM below T_C = 87K, PM above	[111] [116]
$HgCr_2Se_4$	Cr(III), Cr(IV)		43.07 42.97	3.92	0	1.4 4.2	Semiconductor, FM below T_C = 105K, PM above	[111] [116]
$HgCr_2S_4$	Cr(III), Cr(IV)		45.68			1.4	Semiconductor, AFM below T_N = 22K, PM above	[111]

				3.80				[110]
$Cr_{0.33}NbSe_2$ (2 inequivalent sites)	Cr(III), Cr(IV) 2.3μ_B/Cr		49.98 53.44	2.48 7.64		4.2	Semiconductor, FM below T_C = 82K, PM above	[7]
$Cr_{0.5}NbSe_2$	Cr(III), Cr(IV) 1.9μ_B/Cr		54.31	7.64		4.2	Semiconductor, AFM below T_N = 53K, PM above	[7]
$Cr_{0.33}NbS_2$ (2 inequivalent sites)	Cr(III), Cr(IV) 2.82μ_B/Cr 2.1μ_B/Cr		65.3-66.6, 49.9-50.2 55.5-56.8 38.3-38.7	2.46 2.16 2.46 2.16		4.2 77	Semiconductor, FM below T_C = 127K, PM above	[117]
CrO_2 (1 site but 2 frequencies, see text in Section 4.5)	Cr(IV) 1.94μ_B/Cr		26.5, 37.2 26.3, 37.1 26.4, 37.1 25.3, 36.2 25.3, 35.9	1.03 [a] 1[a]	0	4.2 4.2 6.5 77 77	Half metal, FM below T_C = 395K PM above	[19] [21] [17] [21] present work
Li_2CrO_4 (dihydrate)	Cr(VI)	-62**		4.00	0.30	295	Insulator, diamagnetic	[22]
Li_2CrO_4 (anhydrous)	Cr(VI)	-17**		1.80	0.15	295	Insulator, diamagnetic	[22]
K_2CrO_4	Cr(VI)	-35** -32**		1.76 1.75	0.43 0.40	295 295	Insulator, diamagnetic	[22] [44]
Rb_2CrO_4	Cr(VI)	-24**		1.28	0.80	295	Insulator, diamagnetic	[22]
Cs_2CrO_4	Cr(VI)	-19** -22**		1.23 1.17	0.23 0	295	Insulator, diamagnetic	[22] [44]
Ag_2CrO_4	Cr(VI)	188**		4.10	0.28	295	Insulator, diamagnetic	[22]

$(NH_4)_2CrO_4$	Cr(VI)	0		3.1	0.58	295	Insulator, diamagnetic	present work
$MgCrO_4$ (dihydrate)	Cr(VI)	-67**		2.62	0.38	295	Insulator, diamagnetic	[22]
$CaCrO_4$	Cr(VI)	-117**		4.55	0	295	Insulator, diamagnetic	[22]
$SrCrO_4$	Cr(VI)	-27**		5.0	0.68	295	Insulator, diamagnetic	[22]
$BaCrO_4$	Cr(VI)	0 -47**		4.9 5.00	0.16 0.14	295 295	Insulator, diamagnetic	present work [22]
$PbCrO_4$	Cr(VI)	68**		4.4	0.85	295	Insulator, diamagnetic	[22]
$Cs_2Cr_2O_7$	Cr(VI)	-17**		7.25	0.30	295	Insulator, diamagnetic	[22]
$\alpha K_2Cr_2O_7$ (2 inequivalent sites)	Cr(VI)	-22** -67**		7.48 8.28	0.30 0.21	295	Insulator, diamagnetic	[22]

* shift with respect to saturated aqueous solution of alkali chromate (Na_2CrO_4 or $(NH_4)_2CrO_4$)

** originally reported with respect to $Cr(CO)_6$ in chloroform solution (the difference is −1797 ppm, i.e., aq $Cr(CO)_6$ is 0 ppm wrt itself or −1797 ppm wrt aq Na_2CrO_4)

[a] no singularities, upper limit estimate of C_Q using fwhm of Gaussian peak as Δ

[b] extrapolation from field dependent data using $\gamma = 2.406$ MHz/T

[c] Ding *et al.* [82] estimate a value for ν_Q but it appears to be inconsistent with the spectrum.

[d] extrapolation to 0 K.

The reader should consult the references to ascertain XRD structure, phase purity, annealing state, and other experimental factors.

Table 5. ^{53}Cr center-line zero applied field magnetic resonance frequency data $\nu_{zf}(T)$ modelled using Bloch spin wave theory.

Compound	Bloch spin wave formulation $\nu_{zf} = \nu_{zf}(0) - c(\mathbf{T/T_{Crit}})^{3/2}$	R^2 goodness of fit	Valence	Critical Transition (Néel or Curie) Temperature T_{Crit} (K)	Spin Wave Stiffness D (meV Å^2)	Reference
$Dy_{0.2}Er_{0.8}CrO_3$	$\nu_{zf} = 74.401 - 32.371(\mathbf{T/T_{Crit}})^{3/2}$	0.995	d^3 Cr(III) ^{oct}	141	34.8	[71]

Cr_2O_3	$\nu_{zf} = 70.985 - 27.436(\mathbf{T/T_{Crit}})^{3/2}$	0.996	d^3 Cr(III) ^{oct}	308	76.3	present work
$MnCr_2O_4$	$\nu_{zf} = 66.657 - 5.198(\mathbf{T/T_{Crit}})^{3/2}$	0.990	d^3 Cr(III) ^{oct}	41	39.7	[96]
$CuCr_2O_4$	$\nu_{zf} = 63.254 - 8.343(\mathbf{T/T_{Crit}})^{3/2}$	0.985	d^3 Cr(III) ^{oct}	135	88.7	[98]
$CrCl_3$	$\nu_{zf} = 63.111 - 39.731(\mathbf{T/T_{Crit}})^{3/2}$	0.999	d^3 Cr(III) ^{oct}	16.8	4.7	[2,136]
Cr_3As_2	$\nu_{zf} = 58.621 - 14.110(\mathbf{T/T_{Crit}})^{3/2}$	0.904	d^3 Cr(III) ^{oct}	243	164	[103]
$CrBr_3$	$\nu_{zf} = 58.229 - 20.265(\mathbf{T/T_{Crit}})^{3/2}$	0.998	d^3 Cr(III) ^{oct}	37	18.4	[1]
$NaCrS_2$	$\nu_{zf} = 54.072 - 12.092(\mathbf{T/T_{Crit}})^{3/2}$	0.988	d^3 Cr(III) ^{oct}	17	8.0	[102]
$FeCr_2S_4$	$\nu_{zf} = 51.381 - 14.145(\mathbf{T/T_{Crit}})^{3/2}$	0.988	d^3 Cr(III) ^{oct}	180	107	[99]
CrI_3	$\nu_{zf} = 49.596 - 15.368(\mathbf{T/T_{Crit}})^{3/2}$	0.987	d^3 Cr(III) ^{oct}	68	32.5	[3]
$ZnCr_2Se_4$	$\nu_{zf} = 46.657 - 11.115(\mathbf{T/T_{Crit}})^{3/2}$	0.988	d^3 Cr(III) ^{oct}	20	14.1	[6]
$K_2Cr_8O_{16}$			mixed valence	180		[19]
Sites A and B	$\nu_{zf} = 46.484 - 23.074(\mathbf{T/T_{Crit}})^{3/2}$	0.998	d^2 Cr(IV) and		142	
Site C	$\nu_{zf} = 42.963 - 21.332(\mathbf{T/T_{Crit}})^{3/2}$	0.998	d^3 Cr(III)		151	
$CdCr_2Se_4$	$\nu_{zf} = 44.179 - 20.103(\mathbf{T/T_{Crit}})^{3/2}$	NA	mixed valence d^2 Cr(IV) and d^3 Cr(III)	129	65	[111,116]
$CuCr_2S_4$	$\nu_{zf} = 40.188 - 21.756(\mathbf{T/T_{Crit}})^{3/2}$	0.997	mixed valence d^2 Cr(IV) and d^3 Cr(III)	420	137	[112,113]
CrO_2 ν_{high}	$\nu_{zf} = 37.038 - 8.681(\mathbf{T/T_{Crit}})^{3/2}$	0.993	d^2 Cr(IV) ^{tet}	395	127	[15]
CrO_2 ν_{high}	$\nu_{zf} = 37.068 - 9.882(\mathbf{T/T_{Crit}})^{3/2}$	0.996			113	present work
ν_{low}	$\nu_{zf} = 26.407 - 10.151(\mathbf{T/T_{Crit}})^{3/2}$	0.982			90.4	present work
Cr_3AsN	$\nu_{zf} = 14.504 - 2.397(\mathbf{T/T_{Crit}})^{3/2}$	0.992	d^6 Cr(0) low spin	255	410	[78]

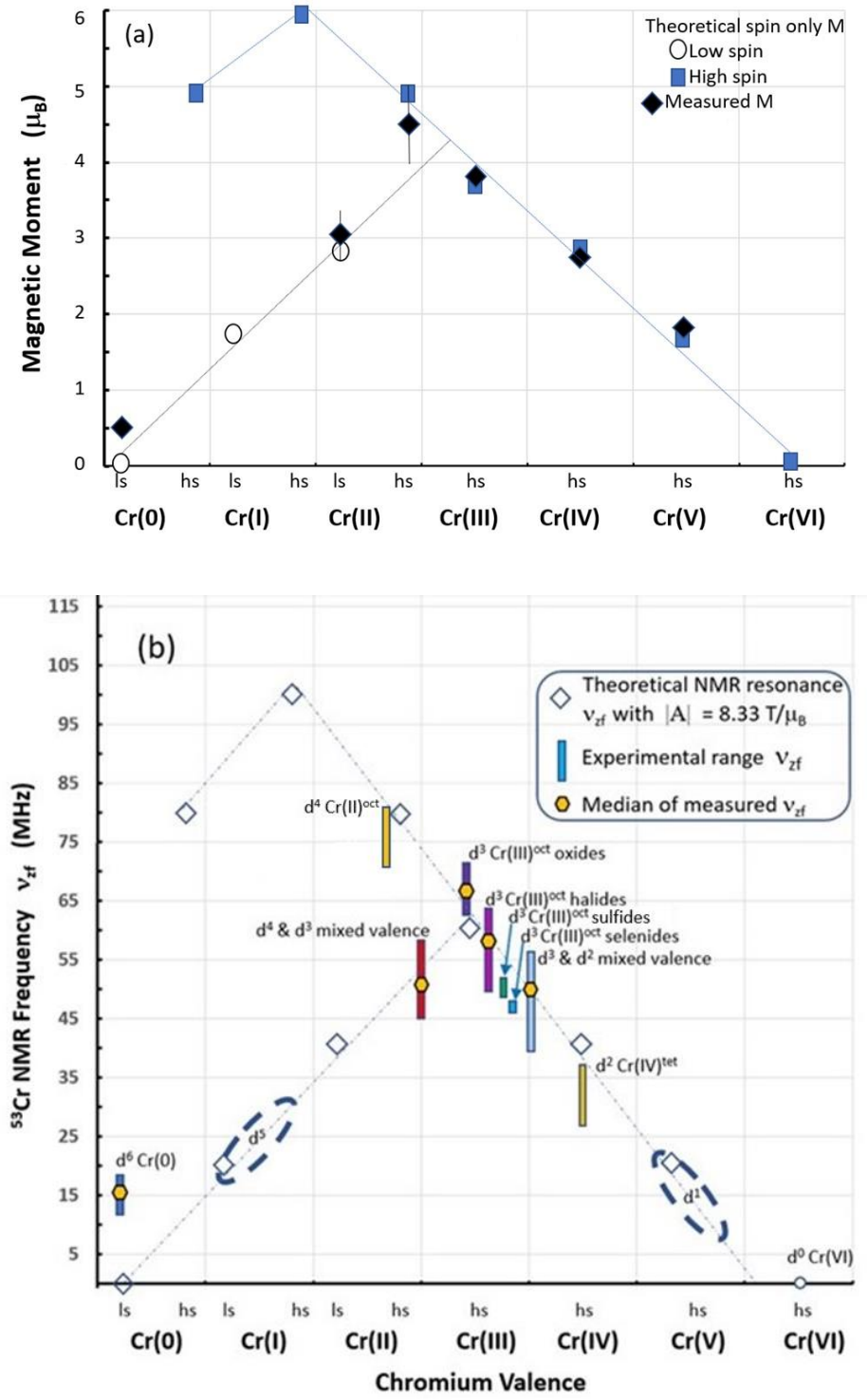

Figure 7. (a) Magnetic moment as a function of valence for Cr compounds, and (b) the ^{53}Cr zero applied field magnetic resonance frequency near 0 K as a function of Cr valence.

Hence the internal field data near 0 K can be used to gain knowledge of the local internal field at the ^{53}Cr nucleus in the ground state and can be used to understand the valence state. As discussed in the next section, the temperature dependence of the magnetic resonance central frequency for systems adequately modelled by spin wave theory can also prove useful for understanding magnetic stability.

4.7.2 Zero applied field NMR as a function of temperature

As discussed in Section 4.5, the internal field data as a function of temperature well below the critical temperature region (< $0.8T_{Crit}$) may be modelled using the Bloch $T^{3/2}$ relation which is valid for any crystal structure [135]. **Table 5** provides data for Cr compounds (in addition to CrO_2 and Cr_2O_3) where the magnetization (antiferromagnetic, ferromagnetic and ferrimagnetic) can be modelled to a first approximation by Bloch spin wave theory. The magnetic resonance data for these sixteen compounds are summarized in **Figure 8**.

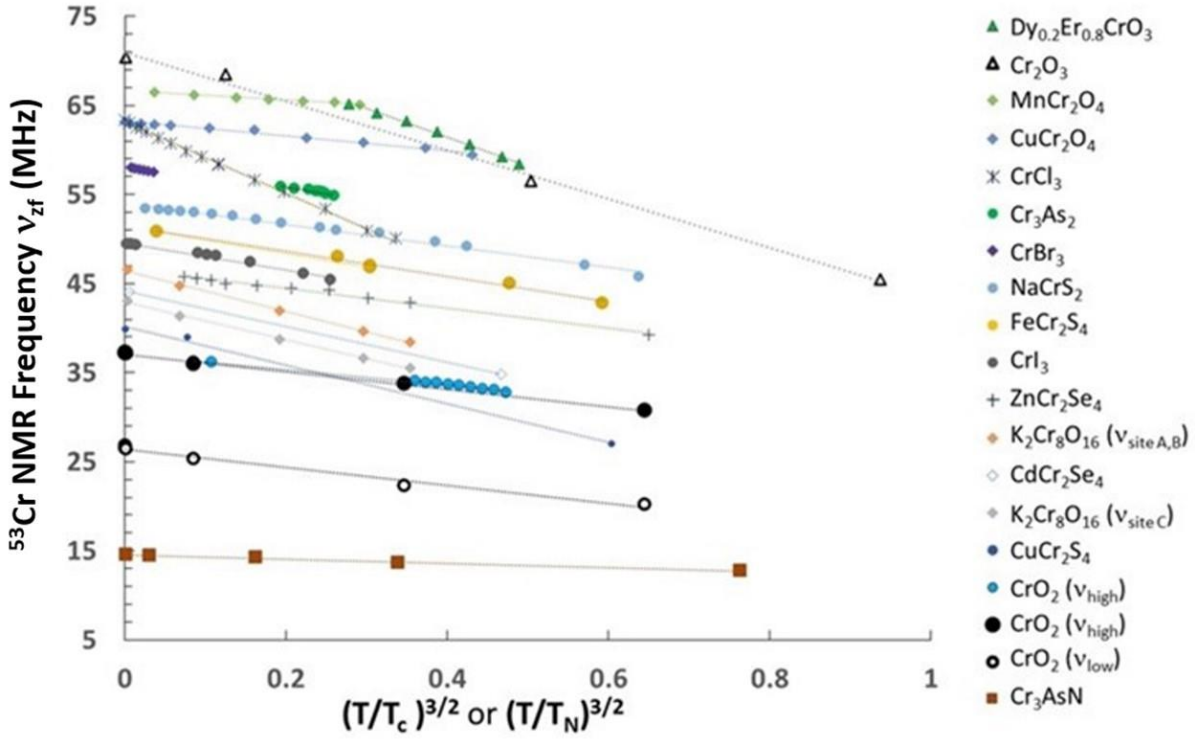

Figure 8. Bloch spin wave theory applied to internal field NMR center-line frequency, ν_{zf}, data for sixteen compounds using data adapted from the literature cited in **Table 5**.

Bastow *et al.* [137,138] have shown that experimental Debye-Waller factors for a range of crystalline solids also have a $T^{3/2}$ dependency attributed to the variation of the mean square amplitude of vibration of atoms in crystals over a temperature range from the Debye temperature to close to the melting point. As the data in **Figure 8** are for crystalline compounds far below their Debye temperature, the $T^{3/2}$ dependency can be attributed to the fundamental magnetization behavior described by spin wave theory [11]. The goodness of fit values for these data (**Table 5**, [35]) support further investigation of parameters that can be extracted from the Bloch spin wave relationship for the temperature dependence of the magnetization M at $T < T_{Crit}$ as follows [11,135]:

$$M(T)/M(0) = 1 - a_{3/2}(T)^{3/2} \qquad \text{(Eq. 8)}$$

where $a_{3/2}$ has units of $K^{-3/2}$ and is related to the spin stiffness in zero field, D, using the relationship [135]:

$$a_{3/2} = [2.612(g\mu_B)/(\rho M(0))][k_B/(4\pi D)]^{3/2} \quad \text{(Eq. 9)}$$

where g is the dimensionless Lande g factor, ρ is the density in kg/m^3, $\mu_B = 9.27\times10^{-24}$ J/T, $k_B = 8.617\times10^{-5}$ eV/K, and M(0) is the saturation magnetization at 0 K in J/(Tkg). Rewriting Eq. 8 using the relationship between ν_{zf} and M in Eq. 7 and as presented in **Table 5**, gives

$$\nu_{zf}(T) = \nu_{zf}(0) - c(T/T_{crit})^{3/2} \quad \text{(Eq. 10)}$$

where $\nu_{zf}(0)$ is related to the electronic and magnetic properties, and the slope, $c = a_{3/2}\nu_{zf}(0)(T_{crit})^{3/2}$ with the parameter $a_{3/2}$ related to the lattice geometry and magnetic exchange interaction. Since the data are well fitted to the Bloch $T^{3/2}$ relationship, the spin wave excitation gap can be considered negligible [139]. For the sixteen compounds in **Table 5**, values of $a_{3/2}$, density, and low temperature saturation magnetization are given in [35] and used to calculate spin stiffness D. **Figure 9 (a)** shows that the low temperature saturation magnetization values reported in the literature for these Cr compounds as compared to values calculated from $\nu_{zf}(0)$ are in very good agreement, in support of the validity of Eq. 7 for these compounds. As shown in **Table 5**, the compound with the highest slope c, $CrCl_3$, has the lowest spin stiffness of 4.7 meV Å^2. The compound with the lowest slope c, Cr_3AsN, has the highest spin stiffness of 410 meV Å^2. Only two of the sixteen compounds have published values for D from magnetic measurements or theory, and these are CrI_3, D = 27±6 meV Å^2 [139], where the error bars of ~20% reflect the population standard deviation for different samples, and CrO_2, D = 91 meV Å^2 [140]. Both published D values for these ferromagnetic compounds compare well (within ~15%) with the values calculated from the internal field data as shown in **Table 5**. Calculation of D from magnetization data for the antiferromagnetic semiconductor $ZnCr_2Se_4$ [141] gives D = 13.7 meV Å^2 within 3 % of the value D = 14.1 meV Å^2 calculated from the internal field data. Calculation of D from magnetization data for the antiferromagnetic semiconductor Cr_2O_3 [69] gives D = 61.2 meV Å^2 within 20 % of the value D = 76.3 meV Å^2 calculated from the internal field data. The D value calculated for Cr_3AsN can be compared with D values for other metals. Lowde [142] has published D values for the metallic CrFe system in the range 100-300 meV Å^2, and Lewis [143] has reported D = 284±40 meV Å^2 for metallic ferrimagnetic Pt_3Cr; all values are the same order of magnitude as the value calculated for metallic ferrimagnetic Cr_3AsN in **Table 5**, noting that an analysis of published magnetic measurements of Cr_3AsN [78] suggests D = 229 meV Å^2 which is ~40% lower than the value from internal field magnetic resonance data. Thus, the values of D in **Table 5** appear reasonable for ferro-, ferri-, and antiferromagnetic chromium compounds, and this tabulation can be useful for comparison with magnetic measurements or density functional approaches to the calculation of spin stiffness in Cr alloys and compounds. **Figure 9 (b)** shows the relationship between spin stiffness and critical transition temperature for the Cr(III) d^{3oct} subset of compounds from **Table 5**. This relationship, D = (0.45 meV Å^2/K)T_{Crit} resembles that reported for a family of magnetic cobalt Heusler alloys of D = (0.36 meV Å^2/K)T_{Crit} [144]. The relationship between spin stiffness D and T_{crit}, for all Cr alloys and compounds from **Table 5**, is D = (0.37 meV Å^2/K)T_{Crit} [35].

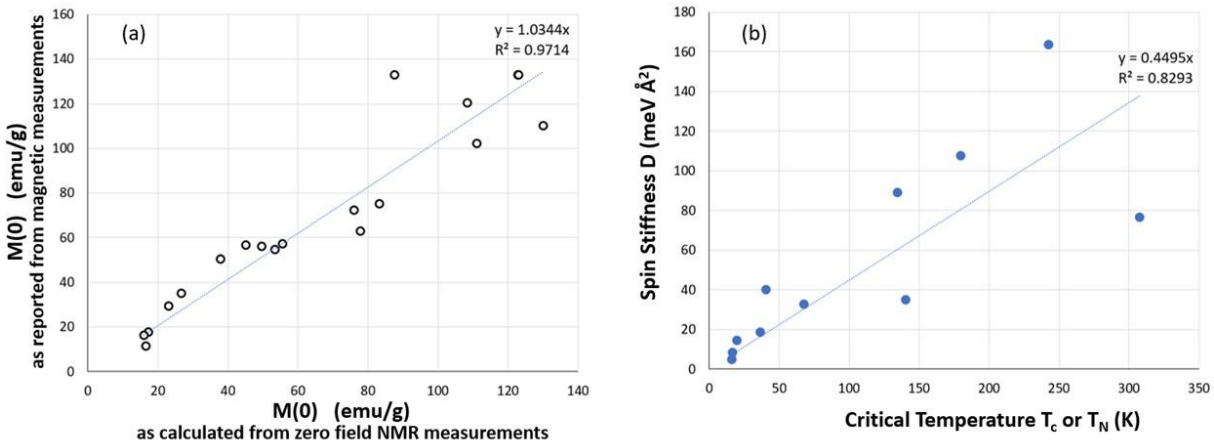

Figure 9. (a) Comparison of spontaneous magnetization at low temperature as reported from magnetic measurements and as calculated from internal field magnetic resonance data. (b) Spin stiffness and critical temperature for the d^3 $Cr(III)^{oct}$ compounds in Table 5, including ferromagnetic, antiferromagnetic, and ferrimagnetic compounds.

4.7.3 External field NMR

The second focus of Section 4.7 is inclusive of non-magnetic Cr compounds. Two recent solid-state NMR reviews have commented on the challenges of recording ^{53}Cr solid-state NMR spectra, citing only three reports on ^{53}Cr NMR of the diamagnetic octahedral Cr(0) d^6 compound $Cr(CO)_6$ and diamagnetic tetrahedral Cr(VI) d^0 chromates and dichromates [23,24]. The comprehensive up to date summary of magnetic and non-magnetic compounds presented in **Table 4** permits an expanded discussion of the ^{53}Cr solid-state NMR characteristics of interest to experimentalists and theorists. The range of C_Q observed for these compounds (Cr(0), Cr(II), Cr(III), Cr(IV), mixed valence, and Cr(VI)) is 0.2 MHz $\leq C_Q \leq$ 8.28 MHz. The range reported in diamagnetic alkali earth chromate and dichromate compounds alone is 1.28 MHz $\leq C_Q \leq$ 8.28 MHz [22,44], all with Cr(VI) electron configuration. Some generalizations can be made based on the data in **Table 4** – the Cr compounds with $C_Q \leq \sim 1$ MHz tend to be semiconductors. Insulating compounds have C_Q values ranging from 1.3 to 4.4 MHz. The compounds with $C_Q > 4$ MHz tend to be semiconductors and metals. These observations provide some general guidelines for the likely magnitude of C_Q to be found in such materials. These are some of the parameters that could feature in an NMR crystallography approach to detailed local structural characterisation.

As discussed in Section 4.1, DFT calculations of Knight shifts and chemical shifts in transition metal compounds require orbital and spin contributions to accurately reproduce the experimental values. Knight shifts for the ^{53}Cr compounds in **Table 4** range from –9982 to 6990 ppm and can be temperature dependent. As shifts are reported relative to the Cr ion in solution, ionic compounds typically have shifts near 0 ppm, i.e. –100 ppm $< \delta <$ 100 ppm (see **Figure 10**). As $(CO)_6$ is a strong field ligand, the Cr(0) complex $Cr(CO)_6$ is more shielded (–1814 ppm) than the chromate salts. As bonding covalency increases, leading finally to metallic conduction, the shielding also increases and the Fermi contact term dominates the contribution to the shift. As shown in **Table 4**, the present work, to the best of our knowledge, has measured the largest Cr(0) Knight shift (–9982 ppm for CrB_2) for any

chromium-containing metallic material reported to date. **Figure 10** illustrates the range of chemical and Knight shifts for ^{53}Cr alloys and compounds.

The hyperfine coupling constant A, or the core polarization hyperfine field per unpaired valence electron for the 3d transition metal ^{53}Cr, plays a role in the shielding of the nucleus or the magnetic shift away from the Larmor frequency that can be measured by NMR. The exchange polarization between d electrons on the Fermi surface and s electrons in the core orbitals dominates the Knight shift and leads to the large observed Knights shifts in metallic Cr compounds shown in **Figure 10** [31]. In Section 4.7.1 we have shown that the value of |A| of 8.33 T/μ_B reasonably describes Cr alloys across the range of crystal structures. Assuming A is independent of temperature, the Knight shift should be proportional to the magnetic susceptibility, such that a large Knight shift is indicative of a large Pauli spin susceptibility χ_P per Cr atom (Eq. 4). The experimental magnetic susceptibility of CrB_2 at room temperature in the paramagnetic state has been reported in a range from 0.485 to 0.795 (10^{-3} cm^3/mol) [145-148]. Using this range for susceptibility and the measured ^{53}Cr Knight shift value of –0.9982 % reported here, the Clogston-Jaccarino [149] analysis can be applied [35], assuming negligible orbital contribution to the Knight shift and negligible transferred hyperfine field, resulting in a range of values for |A| from 7.0 to 11.5 T/μ_B, in agreement with the treatment presented in Section 4.7.1. *Ab initio* calculation of the magnetic susceptibility for CrB_2 metal in the paramagnetic state suggests that the magnetic susceptibility is dominated by the spin contribution, χ_{spin} = 0.703 (10^{-3} cm^3/mol) in agreement with experimental results [146]. It can be noted that Laskowski and Blaha [37] have calculated the Knight shift and magnetic susceptibility for Cr metal including orbital and spin contributions, with their theoretical values coming within 10% of the measured values. Our results suggest that theoretical calculation of the Knight shift for CrB_2 should be the subject of fruitful future work.

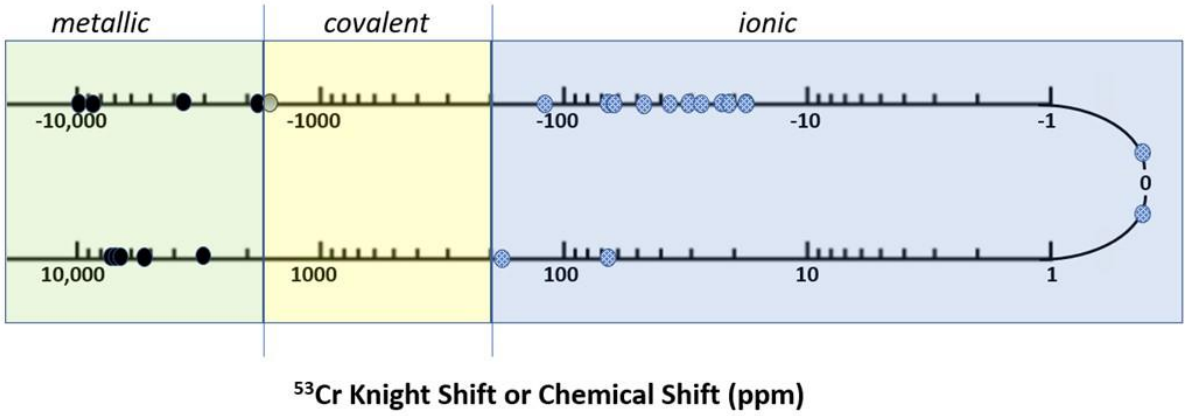

Figure 10. Knight shift or chemical shift for ^{53}Cr compounds from Table 4. Shift is with respect to saturated aqueous solution of alkali chromate (Na_2CrO_4 or $(NH_4)_2CrO_4$).

4.7.4 Hyperfine interactions as a guide to the production of novel materials

A theme of the discussion thus far has been the ability of magnetic resonance to determine parameters that can be useful to check theoretical models and their predictions in magnetic and non-magnetic Cr alloys and compounds. In addition, it is suggested that the hyperfine interactions probed by magnetic resonance are useful guides for the selection and production of novel materials for industrial applications. The multivalent nature of chromium makes for

a variety of stable compounds with diverse magnetic properties. The ability to tune and control room temperature accessible magnetic states makes chromium alloys and compounds prime candidates for quantum engineering devices, and NMR adds to the ways these states can be probed. The results presented here have shown a correlation between the critical transition temperature (T_C or T_N) and the spin stiffness in zero field, D, calculated from magnetic resonance data for Cr alloys and compounds. The local, site specific nature of magnetic resonance as a probe technique means that this approach can be used across a range of valences, including mixed valence, various crystal structures, and ferro-, ferri-, antiferro-magnetic order. D is a measure of the resistance of the spin lattice to thermal disturbance, hence the magnetic resonance parameters enable an indirect test of the robustness of spin polarization in Cr alloys and compounds. The data presented here can also guide the discovery of technologically important ferro-, ferri-, and antiferro- magnetic materials with high critical temperatures and stable properties given the correlations that have been developed here. A number of approximations are involved in the treatment of these compounds using Bloch spin wave theory including (i) dominance of spin rather than spin orbital contributions, (ii) same treatment for all crystal and magnetic structures, (iii) temperature independent and valence independent hyperfine coupling constant, (iv) an isotropic Fermi contact interaction, and (v) a dominant core polarisation contribution to the hyperfine field, such that the treatment points to some key features as drivers of behavior in these systems. With the accumulation of experimental data for training sets, it is hoped that these key features will be able to be investigated using machine learning. Extending this approach, one might speculate what local site properties at chromium could be related directly to the macroscopic properties needed, such as the size of the efg as a characteristic of the local site distortion and the impact on quantum switching. In low-dimensional spin systems, hyperfine fields contribute to decoherence in the system, leading to limitation in the performance of potential quantum devices [126].

5. Summary

This study encompassing new experimental observations and a comprehensive survey of magnetic resonance parameters collected on ^{53}Cr shows it can be quite a receptive nucleus for NMR with an external field or zero field. Therefore ^{53}Cr NMR can be used to characterize a range of important materials including metals, half metals, insulators, semiconductors, ferromagnetic, antiferromagnetic, and diamagnetic materials. The ^{53}Cr solid-state NMR work to date of relevance to the new observations here has been summarized and put into context. The work presented here has established quadrupolar coupling constants and chemical/Knight shifts for the first time for several important compounds. The $T^{3/2}$ behavior of the sublattice magnetization of CrO_2 and Cr_2O_3 measured via ^{53}Cr zero applied field NMR are reported here over a wide temperature range from liquid He temperature to room temperature. The large negative Knight shift of ^{53}Cr in the transition metal intermetallic CrB_2 has been measured. Unexplained lineshapes have been reported here for high purity Cr_2O_3, and these should be the subject of future verification and elucidation. Also, as in the case of AlN, it may take careful single crystal work or enriched specimens or both to pinpoint singularities and C_Q values in some of the Cr compounds discussed here, where only an upper limit on C_Q could be estimated.

The first comprehensive summary of ^{53}Cr NMR interaction parameters for chromium compounds reported from 1961 to 2022 has been tabulated. Here is shown how low temperature internal field central frequencies have been correlated with valence state, and spin stiffness has been calculated for sixteen chromium compounds. The local information provided from ^{53}Cr NMR complements bulk measurements. Therefore, such NMR data can

help determine whether new materials show promising characteristics, and, if one could go further and relate these characteristics directly to site parameters (e.g. shift, anisotropy, efg), then one could have a direct measure of desirable properties. Additional theoretical and computational studies have been suggested based on current gaps in the data for ^{53}Cr NMR parameters. Knowledge of these parameters will enable further progress in understanding and capturing the benefits from electronic and magnetic structure-property-function relationships in Cr compounds.

Acknowledgements

We gratefully acknowledge Aaron Seeber for the XRD scans, Mark Greaves for the SEM, Yesim Gozukara for the DSC, and Justin Kimpton for the research undertaken on the powder diffraction beamline at the Australian Synchrotron, part of ANSTO. Professor Ekaterina Izgorodina is thanked for helpful discussions. Adrian Trinchi and Lyndsey Benson are thanked for their support of the work as the leaders of the Functional Powders team at CSIRO. Sadly, Tim Bastow died during the revision of this manuscript. AJH, KMN, and MES thank Tim for sharing his fascination with chromium and passion for magnetic resonance with them.

Author Contributions

TJB devised the experimental plan, contributed the overall supervision of this work, and performed NMR measurements, data analysis, and co-wrote the manuscript. AJH assisted in data collection and analysis and co-wrote the manuscript. KMN and MES assisted in data analysis and editing of the manuscript.

Competing interests statement: The authors declare no competing interests.

References

[1] A. C. Gossard, V. Jaccarino, and J. P. Remeika, Experimental test of the spin-wave theory of a ferromagnet. Phys. Rev. Lett. 7, 122 (1961).

[2] A. Narath, Nuclear magnetic resonance of Cr^{53} in antiferromagnetic $CrCl_3$. Phys. Rev. Lett. 7, 410 (1961).

[3] A. Narath, Zero-field ^{53}Cr nuclear magnetic resonance in ferromagnetic CrI_3: renormalized spin-wave and Green's-function analysis. Phys. Rev. 140, A854 (1965).

[4] R. G. Barnes and T. P. Graham, Nuclear magnetic resonance in chromium metal. Phys. Rev. Lett. 8, 248 (1962).

[5] R. G. Barnes and T. P. Graham, Néel temperatures of chromium vanadium alloys from NMR measurements. J. Appl. Phys. 36, 938 (1965).

[6] S. Park, S. Kwon, S. Lee, S. Khim, D. Bhoi, C. B. Park, and K. H. Kim, The zero field ^{53}Cr nuclear magnetic resonance interactions in the bond-frustrated helimagnet $ZnCr_2Se_4$ investigated by NMR. Sci. Rep. 9, 16627 (2019).

[7] N. M. Toporova, E. M. Sherokalova, N. V. Selezneva, V. V. Ogloblichev, and N. V. Baranov, Crystal structure, properties and griffiths-like phase in niobium diselenide intercalated with chromium. J. Alloys Compd. 848, 156534 (2020).

[8] E. Garlatti, G. Allodi, S. Bordignon, L. Bordonali, G. A. Timco, R. E. P. Winpenny, A. Lascialfari, R. De Renzi, and S. Carretta, Breaking the ring: ^{53}Cr-NMR on the {Cr_8Cd} molecular nanomagnet. J. Phys. Condens. Matter. 32, 244003 (2020).

[9] F. Bloch, On the theory of ferromagnetism. Z. Physik. 61, 206 (1930).

[10] F. J. Dyson, Thermodynamic behaviour of an ideal ferromagnet. Phys. Rev. 102, 1230 (1956).

[11] C. Kittel, Introduction to Solid State Physics. 2nd Edition Wiley, Ch 15 (1959).

[12] B. Huang, G. Clark, E. Navarro-Moratalla, D. R. Klein, R. Cheng, K. L. Seyler, D. Zhong, E. Schmidgall, M. A. McGuire, D. H. Cobden, W. Yao, D. Xiao, P. Jarillo-Herrero, and X. Xu, Layer-dependent ferromagnetism in a van der Waals crystal down to the monolayer limit. Nature. 546, 270 (2017).

[13] M. Grönke, Synthesis and characterization of layered transition metal trihalides MCl_3 (M = Ru, Mo, Ti, Cr) and CrX_3 (X = Cl, Br, I). Dissertation, BTU Cottbus-Senftenberg, DOI: 10.26127/BTUOpen-5282 (2020).

[14] M. Rubinstein, G. H. Stauss, and J. J. Krebs, Nuclear magnetic resonance of Cr^{53} in antiferromagnetic Cr_2O_3. Phys. Lett. 12, 302 (1964).

[15] H. Yasuoka, H. Abe, A. Hirai, and T. Hashi, Nuclear magnetic resonance of Cr^{53} in ferromagnetic CrO_2. J. Phys. Soc. Japan. 18, 593 (1963).

[16] H. Nishihari, T. Tsuda, A. Hirai, and T. Shinjo, Nuclear magnetic resonance of Cr^{53} in ferromagnetic CrO_2. J. Phys. Soc. Japan. 32, 85 (1972).

[17] J. H. Shim, S. Lee, J. Dho, and D. H. Kim, Coexistence of two different Cr ions by self-doping in half-metallic CrO_2 nanorods. Phys. Rev. Lett. 99, 057209 (2007).

[18] H. Takeda, Y. Shimizu, M. Itoh, M. Isobe, and Y. Ueda, Electronic states of half-metallic chromium oxides probed by ^{53}Cr NMR. J. Phys.: Conf. Ser. 400, 032098 (2012).

[19] H. Takeda, Y. Shimizu, M. Itoh, M. Isobe, and Y. Ueda, Local electronic state in the high-valence hollandite-type chromium oxide $K_2Cr_8O_{16}$ investigated by ^{53}Cr NMR. Phys. Rev. B. 88, 165107 (2013).

[20] H. Takeda, Y. Shimizu, Y. Kobayashi, M. Itoh, T. Jin-no, M. Isobe, Y. Ueda, S. Yoshida, Y. Muraoka, and T. Yokoya, Local electronic state in the half-metallic ferromagnet CrO_2 investigated by site-selective ^{53}Cr NMR measurements. Phys. Rev. B. 93, 235129 (2016).

[21] Y. V. Piskunov, A. F. Sadykov, V. V. Ogloblichev, A. G. Smolnikov, A. P. Gerashenko, and P. Z. Si, Valence state of chromium ions in the half-metallic ferromagnet CrO_2 probed by ^{53}Cr NMR. Phys. Rev. 106, 094428 (2022).

[22] M. A. M. Forgeron and R. E. Wasylishen, A solid-state ^{53}Cr NMR study of chromate and dichromate salts. Magn. Reson. Chem. 46, 206 (2008).

[23] C. Leroy and D. L. Bryce, Recent advances in solid-state nuclear magnetic resonance spectroscopy of exotic nuclei. Prog. Nucl. Magn. Reason. Spectrosc. 109, 160 (2018).

[24] M. E. Smith, Recent progress in solid-state nuclear magnetic resonance of half-integer spin low-γ quadrupolar nuclei applied to inorganic materials. Magn. Reson. Chem. 59, 864 (2021).

[25] B. W. Epperlein, H. Krüger, O. Lutz, A. Nolle, and W. Mayr, ^{53}Cr Fourier transform nuclear magnetic resonance studies. Z. Naturforsch. 30a, 1237 (1975).

[26] B. Nowak, O. J. Żogal, K. Niedźwiedź, M. Tkacz, and Z. Żolnierek, ^{53}Cr Knight shift and magnetic susceptibility of hexagonal $CrH_{0.93}$. Physica B. 193, 102 (1994).

[27] J. Poźniak-Fabrowska, B. Nowak, and M. Tkacz, Magnetic properties of cubic and hexagonal chromium hydrides: a comparison of the magnetic susceptibility with the ^{53}Cr NMR Knight shift. J. Alloys Compd. 322, 82 (2001).

[28] M. Kontani, T. Hioki, and Y. Masuda, Hyperfine fields in an incommensurate antiferromagnetic Cr-Mo alloy system. J. Phys. Soc. Japan. 39, 672 (1975).

[29] M. E. Smith and K. J. D. MacKenzie, Multinuclear solid state NMR of inorganic materials. Pergamon Press Oxford (2002).

[30] M. E. Smith and E. R. H van Eck, Recent advances in experimental solid state NMR methodology for half-integer spin quadrupolar nuclei (Review). Prog. Nucl. Magn. Reson. Spectrosc. 34, 159 (1999).

[31] G. C. Carter, L. H. Bennett, and D. J. Kahan, Metallic shifts in NMR: A review of the theory and comprehensive critical data compilation of metallic materials. Progress in Materials Science Volume 20. Pergamon Press Oxford (1977).

[32] T. J. Bastow, Materials characterisation by nuclear quadrupole interaction. Z Naturforsch. 49a, 320 (1994).

[33] E. A. Turov and M. P. Petrov, Nuclear magnetic resonance in ferro- and antiferromagnets. Halsted Press John Wiley and Sons Inc New York (1972).

[34] C. Meny and P. Panissod, Nuclear magnetic resonance in ferromagnets: Ferromagnetic nuclear resonance; a very broadband approach. Ann. Rep. NMR Spectrosc. 103, 47 (2021).

[35] See Supplemental Material at http://link.aps.org/supplemental... for NMR probe, XRD patterns, SEM image, DSC scans, internal field NMR data, mixed valence data, spin stiffness data, and Clogston-Jaccarino analysis.

[36] T. J. Bastow, M. I. Burgar, and C. Maunders, Electric field gradients in metals: correlation of experimental results with ab initio calculation. Solid State Commun. 122, 629 (2002).

[37] R. Laskowski and P. Blaha, NMR shielding in metals using the augmented plane wave method. J. Phys. Chem. C. 119, 19390 (2015).

[38] P. Blaha, K. Schwarz, G. K. H. Madsen, D. Kvasnicka, and J. Luitz, WIEN2k, an augmented plane wave plus local orbitals program for calculating crystal properties. Vienna University of Technology: Vienna, Austria. ISBN 3-9501031-1-2 (2001).

[39] C. P. Slichter, Principles of Magnetic Resonance, 3rd Edition Springer-Verlag New York (1989).

[40] J. E. Wertz and J. R. Bolton, Electron Spin Resonance. Chapman and Hall New York, Ch 11 (1986).

[41] J. S. Stephens and D. W. J. Cruikshank, A re- investigation of the crystal structure of $(NH_4)_2CrO_4$. Acta Crystallogr. B26, 437 (1970).

[42] A. Lentz, W. Büchele, and H. Schöllhorn, Crystal growth from silica gels and single crystal structure of barium chromate. Cryst. Res. Technol. 21, 827 (1986).

[43] D. Massiot, F. Fayon, M. Capron, I. King, S. Le Calvé, B. Alonso, J-O. Durand, B. Bujoli, Z. Gan, and G. Hoatson, Modelling one- and two-dimensional solid-state NMR spectra. Magn. Reson. Chem. 40, 70 (2002).

[44] D. L. Bryce and R. E. Wasylishen, The first chromium-53 solid-state nuclear magnetic resonance spectra of diamagnetic chromium(0) and chromium(VI) compounds. Phys. Chem. Chem. Phys. 3, 5154 (2001).

[45] M. Bühl, Density-functional computation of ^{53}Cr NMR chemical shifts. Magn. Reson. Chem. 44, 661 (2006).

[46] T. H. Lee, S. J. Kim, E. Shin, and S. Takaki, On the crystal structure of Cr_2N precipitates in high-nitrogen austenitic stainless steel. III. Neutron diffraction study on the ordered Cr_2N superstructure. Acta Crystallogr. B. 62, 979 (2006).

[47] L. M. Corliss, N. Elliot, and J. M. Hastings, Antiferromagnetic structure of CrN. Phys. Rev. 117, 929 (1960).

[48] G. Wang, Theoretical prediction of the intrinsic half-metallicity in surface-oxygen-passivated Cr_2N MXene. J Phys. Chem. C. 120, 18850 (2016).

[49] L. A. O'Dell, Direct detection of nitrogen-14 in solid-state NMR spectroscopy. Prog. Nucl. Magn. Reason. Spectrosc. 59, 295 (2011).

[50]. T. J. Bastow, D. Massiot, and J. P. Coutures, ^{14}N NMR in AlN and BN. Solid State Nucl. Magn. Reson. 19, 241 (1998).

[51] O. E. O. Zeman, I. L. Moudrakovski, C. Hartmann, S. Indris, and T. Bräuniger, Local electronic structure in AlN studied by single-crystal ^{27}Al and ^{14}N NMR and DFT calculations. Molecules. 25, 469 (2020).

[52] T. Tanaka, H. Nozaki, E. Bannai, Y. Ishizawa, S. Kawai, and T. Yamane, Preparation and properties of CrB_2 single crystals. J. Less-Common Met. 50, 15 (1976).

[53] A. Bauer, A. Regnat, C. G. F. Blum, S. Gottlieb-Schönmeyer, B. Pedersen, M. Meven, S. Wurmehl, J. Kuneš, and C. Pfleiderer, Low-temperature properties of single-crystal CrB_2. Phys. Rev. B. 90, 064414 (2014).

[54] C. N. Guy and A. A. Uraz, The chromium-boron system. J. Less-Common Met. 48, 199 (1976).

[55] K. Schwarz, H. Ripplinger, and P. Blaha, Electric field gradient calculations on various borides. Z. Naturforsch. 51a, 527 (1996).

[56] R. J. Schoenberger and R. G. Barnes, NMR study of the antiferromagnetic transition in $V_xCr_{1-x}B_2$. AIP Conf. Proc. 5, 392 (1972).

[57] C. N. Guy, The electronic properties of chromium borides. J. Phys. Chem. Solids. 37, 1005 (1976).

[58] X. Y. Chong, Y. H. Jiang, R. Zhou, and J. Feng, Elastic properties and electronic structures of Cr_xB_y as superhard compounds. J. Alloys Compd. 610, 684 (2014).

[59] R. G. Barnes, Nuclear magnetic resonance in the non-cubic metals. In Magnetic Resonance. ed. C. K. Coogan. Plenum Press (1970).

[60] A. H. Silver and T. Kushida, Nuclear magnetic resonance in transition-metal diborides, J. Chem. Phys. 38, 865 (1963).

[61] R. G. Barnes and R. B. Creel, Chromium-like antiferromagnetic behavior of CrB_2. Phys. Lett. A. 29, 203 (1969).

[62] S. Funahashi, Y. Hamaguchi, T. Tanaka and E. Bannai, Helical magnetic structure in CrB_2. Solid State Commun. 23, 859 (1977).

[63] Y. Wang, X. Jiang, Y. Wang, and J. Zhao, Ferromagnetic Dirac half-metallicity in transition metal embedded honeycomb borophene. Phys. Chem. Chem. Phys. 23, 17150 (2021).

[64] M. Li, Y. Wang, A. Chen, A. Naidu, B. S. Napier, W. Lia, C. L. Rodriguez, S. A. Crooker, and F. G. Omenetto, Flexible magnetic composites for light-controlled actuation and interfaces. PNAS. 115, 8119 (2018).

[65] S. He, P. Zhou, Y. Yang, W. Wanga, and L. Z. Sun, 1T-CrO_2 monolayer: a high-temperature Dirac half-metal for high-speed spintronics. Nanoscale Adv. 3, 3093 (2021).

[66] T. J. Bastow, M. A. Gibson, and C. T. Forwood, ^{47,49}Ti NMR: hyperfine interactions in oxides and metals. Solid State Nucl. Magn. Reson. 12, 201 (1998).

[67] G. F. Lynch, S. L. Segel, and M. Sayer, Nuclear magnetic resonance of polycrystalline VO_2. J. Magn. Res. 15, 8 (1974).

[68] B. N. Brockhouse, Antiferromagnetic structure in Cr_2O_3. J. Chem. Phys. 21, 961 (1953).

[69] L. M. Corliss and J. M. Hastings, Magnetic structure studies at Brookhaven National Laboratory. J. Phys. (Paris). 25, 557 (1964).

[70] L. M. Corliss, J. M. Hastings, R. Nathans, and G. Shirane, Magnetic structure of Cr_2O_3. J. Appl. Phys. 36, 1099 (1965).

[71] A. S. Karnachev, M. M. Lukina, and E. E. Solov'ev, Magnetic phases and quadrupolar effects in rare-earth orthochromites. Fiz. Nizk. Temp. [Sov. J. Low Temp. Phys.]. 21, 617 (1995).

[72] Johnson Matthey Magnetic Susceptibility Balance Instruction Manual, Issue 3, ECN 306, Appendix C, 10th March (2004).

[73] J. C. Slater, Atomic radii in crystals. J. Chem. Phys. 41, 3199 (1964).

[74] R. D. Shannon, Revised effective ionic radii and systematic studies of interatomic distances in halides and chalcogenides. Acta Crystallogr. A32, 751 (1976).

[75] T. L. Daulton and B. J. Little, Determination of chromium valence over the range Cr(0) - Cr(VI) by electron energy loss spectroscopy. Ultramicroscopy. 106, 561 (2006).

[76] F. Farges, Chromium speciation in oxide-type compounds: application to minerals, gems, aqueous solutions and silicate glasses. Phys. Chem. Miner. 36, 463 (2009).

[77] S. M. Dubiel and H. Lütgemeier, ^{53}Cr site hyperfine fields in iron-rich Fe-Cr alloys. Phys. Lett. A. 84A, 396 (1981).

[78] T. Waki, K. Takao, Y. Tabata, H. Ohta, T. Yajima, Z. Hiroi, and H. Nakamura, Possible itinerant-electron canted antiferromagnetism in tetragonal antiperovskite Cr_3AsN. J. Phys. Soc. Japan. 86, 104706 (2017).

[79] A. Narath and H. T. Weaver, Impurity nuclear magnetic resonance shifts and spin-lattice relaxation rates in Al:V, Al:Cr, and Al:Mn. Phys. Rev. Lett. 23, 233 (1969).

[80] A. Narath, Magnetic hyperfine interaction studies of magnetic impurities in metals. Crit. Rev. Solid State Mater. Sci. 3, 1 (1972).

[81] K. Le Dang, P. Veillett, and P. J. Walker, Nuclear magnetic resonance studies of ^{53}Cr in a single crystal of Rb_2CrCl_4. J. Phys. C. 10, 4593 (1977).

[82] Q-P. Ding, S. Pakhira, N. S. Sangeetha, E. H. Krenkel, E. I. Timmons, M. A. Tanatar, R. Prozorov, D. C. Johnston, and Y. Furukawa, Itinerant G-type antiferromagnet $SrCr_2As_2$ studied by magnetization, heat capacity, electrical resistivity, and NMR measurements. Phys. Rev. B. 105, 134408 (2022).

[83] M. Yamaguchi and T. Hashimoto, Magnetic properties of Cr_3Te_4 in ferromagnetic region. J. Phys. Soc. Japan. 32, 635 (1972).

[84] E. Jedryka, M. Wojcik, and A. Pajaczkowska, NMR investigation in some compounds of the Cr-Te system. Acta Phys. Pol. 52, 773 (1977).

[85] K. Le Dang and P. Veillett, Résonance magnétique nucléaire dans CrTe et Cr_3Te_4. C. R. Acad. Sci. Ser. B. 264, 1154 (1967).

[86] T. Hashimoto and M. Yamaguchi, Magnetic properties of Cr_7Te_8. J. Phys. Soc. Japan. 27, 1121 (1969).

[87] K. Le Dang, Interaction hyperfine des ions du groupe fer dans les composes ferro et ferrimagnetiques. In Magnetic Resonance and Radiofrequency Spectroscopy. Proceedings of the 15th Colloque A.M.P.E.R.E., Grenoble, September 1968. Edited by P. Averbuch North Holland Publishing Co: Amsterdam, 505 (1969).

[88] K. Le Dang, M. Rotter, and R. Krishnan, Hyperfine interaction of Cr^{3+} and Cu^{2+} ions in Cr- and Cu-doped YIG. Phys. Status Solidi A. 12, 569 (1972).

[89] A. G. Smol'nikov, V. V. Ogloblichev, S. V. Verkhovskii, K. N. Mikhalev, A. Y. Yakubovskii, K. Kumagai, Y. Furukawa, A. F. Sadykov, Y. V. Piskunov, A. P. Gerashchenko, S. N. Barilo, and A. V. Shiryaev. ^{53}Cr NMR study of $CuCrO_2$ multiferroic. JETP Lett. 102, 674 (2015).

[90] A. S. Karnachev, Y. I. Klechin, N. M. Kovtun, A. S. Moskvin, E. E. Solov'ev, and A. A. Tkachenko, Spin-flip and nuclear quadrupole interactions in the rare-earth orthochromites $GdCrO_3$. J. Exp. Theor. Phys. 58, 390 (1983).

[91] A. S. Karnachev, T. K. Soboleva, E. E. Solov'ev, and E. P. Stefanovskiĭ, Temperature dependences of magnetization and frequencies of nuclear magnetic resonance in Cr-53 in yttrium and erbium orthochromites. Solid State Phys. 21, 1451 (1979).

[92] A. S. Karnachev, N. M. Kovtun, M. I. Kurkin, E. E. Solov'ev, and A. A. Tkachenko, Quadrupole splitting and nuclear magnetic relaxation in $ErCrO_3$ near a Morin-type phase transition. J. Exp. Theor. Phys. 58, 130 (1983).

[93] A. S. Karnachev, Y. I. Klechin, N. M. Kovtun, A. S. Moskvin, E. E. Solov'ev, and A. A. Tkachenko, NMR investigation of spin flip in $TmCrO_3$. J. Exp. Theor. Phys. 65, 157 (1987).

[94] M. A. Butler, M. Eibschütz, and L. G. van Uitert, ^{53}Cr nuclear magnetic resonance in the rare-earth orthochromites. Phys. Rev. B. 6, 51 (1972).

[95] D. T. Edmonds and D. R. Taylor, An estimate of the zero-point spin deviation in a spin 3/2 antiferromagnet including the transferred hyperfine interaction. Proc. Phys. Soc., London. 91, 356 (1967).

[96] H. Nagasawa and T. Tsushima, Cr^{53} nuclear magnetic resonance in the non-collinear ferrimagnet $MnCr_2O_4$. Phys. Lett. 15, 205 (1965).

[97] D. Y. Yoon, S. Lee, Y. S. Oh, and K. H. Kim, NMR study on the stability of the magnetic ground state in $MnCr_2O_4$. Phys. Rev. B. 82, 094448 (2010).

[98] E. Jo, B. Kang, C. Kim, S. Kwon, and S. Lee, Spin state and orbital ordering in $CuCr_2O_4$ investigated by NMR. Phys. Rev. B. 88, 094417 (2013).

[99] K. Le Dang, Résonance magnétique nucléaire dans $CuCr_2O_4$ et $FeCr_2S_4$. C. R. Acad. Sci. Ser. B. 262, 1555 (1966).

[100] K. Le Dang, M. C. Mery, and P. Veillet, Spin-glass-like behaviour of the mixed spinel systems $Mn_xZn_{1-x}Cr_2O_4$ and $Mn_{0.75}Mg_{0.25}(Cr_{1-y}V_y)_2O_4$, J. Magn. Magn. Mater. 43, 161 (1984).

[101] J. K. Srivasta, K. Le Dang, and P. Veillet, NMR and magnetization studies of the mixed spinel ferrites $Ga_xFe_{1-x}NiCr_{1-y}Al_yO_4$. J. Magn. Magn. Mater. 54-57, 1341 (1986).

[102] S. L. Carr, P. Erdos, W. G. Moulton, and J. Robinson, Nuclear magnetic resonance experiments and theory of the magnetic properties of $NaCrS_2$. Solid State Commun. 7, 1673 (1969).

[103] T. Shinohara and H. Watanabe, Nuclear magnetic resonance in Cr_3As_2. J. Phys. Soc. Japan. 21, 2076 (1966).

[104] C. M. Casadei, L. Bordonali, Y. Furukawa, F. Borsa, E. Garlatti, A. Lascialfari, S. Carretta, S. Sanna, G. A. Timco, and R. E. P. Winpenny, Local spin density in the Cr_7Ni antiferromagnetic molecular ring and ^{53}Cr-NMR. J. Phys. Condens. Matter. 24, 406002 (2012).

[105] E. Micotti, Y. Furukawa, K. Kumagai, S. Carretta, A. Lascialfari, F. Borsa, G. A. Timco, and R. E. P. Winpenny, Local spin moment distribution in antiferromagnetic molecular rings probed by NMR. Phys. Rev. Lett. 97, 267204 (2006).

[106] M. W. Pieper, H. Lütgemeier, and W. Zinn, Double nuclear magnetic resonance in the weak ferromagnet $YCrO_3$. Z. Phys. B. 63, 369 (1986).

[107] H. Takeda, Y. Shimizu, M. Itoh, F. Chikusa-ku, H. Sakurai, and E. Takayama-Muromachi, Magnetic frustration effects in the new colossal magnetoresistance oxide $NaCr_2O_4$. J. Korean Phys. Soc. 62, 1914 (2013).

[108] Z. H. Han, J. I. Budnick, W. A. Hines, B. Dabrowski, S. Kolesnik, and T. Maxwell, Nuclear magnetic resonance study of the enhanced ferromagnetic ordering in polycrystalline $SrRu_{1-x}Cr_xO_3$ ($0 \leq x \leq 0.12$) J. Phys. Condens. Matter. 17, 1193 (2005).

[109] H. Yokoyama, R. Watanabe, and S. Chiba, Nuclear magnetic resonance studies of $CuCr_2Se_4$ and $CuCr_2Te_4$. J. Phys. Soc. Japan. 23, 450 (1967).

[110] V. N. Berzhanskii, I. A. I. Gorbovanov, and S. N. Polulyakh, Nuclear spin resonance of ^{53}Cr in ferromagnetic $CuCr_2S_4$. Phys. Solid State. 47, 502 (2005).

[111] S. B. Berger, J. I. Budnick, and T. J. Burch, Systematics of the hyperfine and exchange interactions in the chromium chalcogenide spinels. Phys. Rev. 179, 272 (1969).

[112] S. B. Berger, T. J. Burch, J. I. Budnick, and L. Darcy, NMR of $CuCr_{2-x}V_xS_4$ spinels. J. Appl. Phys. 42, 1309 (1971).

[113] K. Le Dang, Resonance magnetique nucleaire dans $CoCr_2S_4$ et $CuCr_2S_4$. Solid State Commun. 6, 203 (1968).

[114] G. N. Abelyashev, V. N. Berzhansky, N. A. Sergeev, and Y. V. Fedotov, Multiquantum effects and NMR in magnetically ordered substances. Phys. Lett. A. 133, 263 (1988).

[115] G. N. Abelyashev, V. N. Berzhansky, S. N. Polulyakh, and N. A. Sergeev, Relaxation of spin echo signals of ^{53}Cr nuclei in Ag-doped $CdCr_2Se_4$. Physica B. 292, 323 (2000).

[116] S. B. Berger, J. I. Budnick, and T. J. Burch, NMR of ^{53}Cr and ^{77}Se in ferromagnetic chalcogenide spinels. J. Appl. Phys. 39, 658 (1968).

[117] V. V. Oglobichev, Y. V. Piskunov, and F. B. Mushenok, Magnetic order in the structurally disordered helicoidal magnet $Cr_{1/3}NbS_2$: NMR at ^{53}Cr nuclei. J. Exp. Theor. Phys. 125, 317 (2017).

[118] D. Feldman, H. R. Kirchmayr, A. Schmolz, and M. Velicescu, Magnetic materials analyses by nuclear spectrometry: A joint approach to Mössbauer effect and nuclear magnetic resonance. IEEE Trans. Magn. 7, 61 (1971).

[119] A. C. Gossard, V. Jaccarino, and J. P. Remeika, NMR in domains and walls in ferromagnetic $CrBr_3$. J. Appl. Phys. 31, 1187 (1962).

[120] V. Heine, Hyperfine structure of paramagnetic ions. Phys. Rev. 107, 1002 (1957).

[121] P. W. Anderson, Theory of magnetic exchange interactions: exchange in insulators and semiconductors. J. Phys. C. 14, 99 (1963).

[122] A. J. Freeman and R. E. Watson, Hyperfine interactions in magnetic materials. In Magnetism. ed. G. T. Rado and H. Suhl. Academic Press Vol. IIA, 167 (1965).

[123] K. Schwarz, CrO_2 predicted as a half-metallic ferromagnet. J. Phys. F. 16, L211 (1986).

[124] F. Tran, J. Doumont, L. Kalantari, A. W. Huran, M. A. L. Marques, and P. Blaha, Semilocal exchange-correlation potentials for solid-state calculations: Current status and future directions. J. Appl. Phys. 126, 110902 (2019).

[125] V. Bellini, A. Olivieri, and F. Manghi, Density-functional study of the Cr8 antiferromagnetic ring. Phys. Rev. B. 73, 184431 (2006).

[126] F. Troiani, V. Bellini, and M. Affronte, Decoherence induced by hyperfine interactions with nuclear spins in antiferromagnetic molecular rings. Phys. Rev. B. 77, 054428 (2008).

[127] B. Budick, R. J. Goshen, S. Jacobs, and S. Marcus, Core polarization in Cr^{53}. Phys. Rev. 144, 103 (1966).

[128] J. M. Friedt and J. P. Sanchez, Origin of the magnetic hyperfine field transferred at iodine in ferromagnetic CrI_3. J. Phys. C. 11, 3731 (1978).

[129] S. Blugel, H. Akai, R. Zeller, and P. H. Dederichs, Hyperfine fields of 3d and 4d impurities in nickel. Phys. Rev. B. 35, 3271 (1987).

[130] P. H. Dederlichs, R. Zeller, H. Akai, and H. Ebert, Ab-initio calculations of the electronic structure of impurities and alloys of ferromagnetic transition metals. J. Magn. Magn. Mater. 100, 241 (1991).

[131] C. Zener, Interaction between the d shells in the transition metals. Phys. Rev. 81, 440 (1951).

[132] C-Y. Yang, L. Pan, A. J. Grutter, H. Wang, X. Che, Q. L. He, Y. Wu, D. A. Gilbert, P. Shafer, E. Arenholz, H. Wu, G. Yin, P. Deng, J. A. Borchers, W. Ratcliff II, and K. L. Wang, Termination switching of antiferromagnetic proximity effect in topological insulator. Sci. Adv. 6, eaaz8463 (2020).

[133] Y. Tokura, K. Yasuda, and A. Tsukazaki, Magnetic topological insulators. Nat. Rev. Phys. 1, 126 (2019).

[134] S. Cottinier, B. De Vries, J. Meersschaut, and M. Rots, What density-functional theory can tell us about the spin-density wave in Cr. J. Phys. Condens. Matter. 14, 3275 (2002).

[135] F. Keffer, Spin waves. In Ferromagnetism. ed. H. P. J. Wijn. Springer-Verlag Berlin Heidelberg (1966).

[136] A. Narath, Low-temperature sublattice magnetization of antiferromagnetic $CrCl_3$. Phys. Rev. 131, 1929 (1963).

[137] T. J. Bastow, S. L. Mair, S. W. Wilkins, Empirical $T^{3/2}$ law for atomic thermal vibration parameters. J. Appl. Phys. 48, 494 (1977).

[138] T. J. Bastow, $T^{3/2}$ dependence of the high temperature electrical resistivity of metals. Phys. Lett. 60A, 487 (1977).

[139] Z. Shu and T. Kong, Spin stiffness of chromium-based van der Waals ferromagnets. J. Phys. Condens. Matter. 33, 195803 (2021).

[140] H. Liu, R. K. Zheng, Y. Wang, H. L. Bai, and X. X. Zhang, Transport and magnetotransport properties of cold-pressed CrO_2 powder. Phys. Status Solidi A. 202, 144 (2005).

[141] F. Yokaichiya, A. Krimmel, V. Tsurkan, I. Margiolaki, P. Thompson, H. N. Bordallo, A. Buchsteiner, N. Stüßer, D. N. Argyriou, and A. Loidl, Spin-driven phase transitions in

$ZnCr_2Se_4$ and $ZnCr_2S_4$ probed by high-resolution synchrotron x-ray and neutron powder diffraction. Phys. Rev. B. 79, 064423 (2009).

[142] R. D. Lowde, M. Shimizu, M. W. Stringfellow, and B. H. Torrie, Density of states effects in the magnetic stiffness of 3d-3d transition metal alloys. Phys. Rev. Lett. 14, 698 (1965).

[143] B. G. Lewis, The magnetic properties of some pseudo-binary platinum–chromium–manganese alloys. PhD Thesis Loughborough University. https://hdl.handle.net/2134/13148 (1974).

[144] R. Y. Umetsu, A. Okubo, A. Fujita, T. Kanomata, K. Ishida, and R. Kainuma, Spin wave stiffness constants of half-metallic ferromagnets Co_2YZ (Y = Cr, Mn, and Fe, Z = Ga, Al, and Si) Heusler alloys. IEEE Trans. Magn. 47, 2451 (2011).

[145] J. Castaing, P. Costa, M. Hertier, and P. Lederer, Spin fluctuation effects in nearly antiferromagnetic vanadium and chromium diborides. J. Phys. Chem. Solids. 33, 533 (1972).

[146] G. E. Grechnev, A. V. Fedorchenko, A. V. Logosha, A. S. Panfilov, I. V. Svechkarev, V. B. Filippov, A. B. Lyashchenko, and A. V. Evdokimova, Electronic structure and magnetic properties of transition metal diborides. J. Alloys Compd. 481, 75 (2009).

[147] G. Balakrishnan, S. Majumdar, M. R. Lees, and D. McK. Paul, Single crystal growth of CrB_2 using a high-temperature image furnace. J. Cryst. Growth. 274, 294 (2005).

[148] L. Leyarovska and E. Leyvarovski, A search for superconductivity below 1 K in transition metal borides. J. Less-Common Met. 67, 249 (1979).

[149] A. M. Clogston and V. Jaccarino, Susceptibilities and negative Knight shifts of intermetallic compounds. Phys. Rev. 121, 1357 (1961).